system (CNS) [12–14]. When activated by a developmental cue, the Hippo core Mst1/2 kinases activate the Lats1/2 kinases, which in turn phosphorylate and negatively regulate the transcriptional cofactor Yap. Control of Yap in this way modulates the transcription of many genes required for tissue-specific cell differentiation [15].

The importance of the Hippo pathway in retinogenesis has been revealed by studies in mice and zebrafish. For example, gene knockout mice lacking Sav1, a component of the Hippo pathway, showed impaired organization of the retinal epithelium during neurogenesis [16]. In a different study, forced expression of Yap in the developing mouse retina led to RPC proliferation and inhibition of retinal differentiation [11]. In zebrafish, knockdown of Yap decreased progenitor cell populations in the CNS, including in the eye [17]. These observations suggest that the Hippo pathway is essential for controlling the balance of self-renewal and differentiation in developing RPCs. However, the precise molecular mechanism by which the Hippo pathway regulates the differentiation of specific types of retinal neurons has remained obscure. In particular, there is little information on the target retinal TF(s) activated downstream of the Hippo-Yap pathway. In this study, we show that the TF Rx1, a novel interacting partner of Yap, is a missing piece of this puzzle and contributes to retinal photoreceptor cell differentiation regulated by the Hippo-Yap pathway. We propose a model in which Yap regulates the timing of photoreceptor cell differentiation by suppressing Rx1-mediated transactivation of the *otx*, *crx* and *rhodopsin* genes.

Results

Mst2 is Required for Early Embryogenesis in Zebrafish

To unravel the role of Hippo signaling in early zebrafish development, we first examined whether zebrafish *mst* functions during early embryogenesis. We performed BLAST searches with human *MST1* and *MST2* genes to predict the sequence of zebrafish *mst* cDNA and found that the zebrafish has only one *mst2* ortholog. The predicted amino acid sequence of the protein encoded by the zebrafish *mst2* gene is approximately 90% identical to the sequences of the human and mouse Mst2 proteins, and contains the evolutionarily conserved autophosphorylation site and SARAH domain that are important for Mst activation (Fig. S1A). A phylogenetic analysis confirmed that the zebrafish *mst2* gene was clustered with those of several vertebrate species, including teleosts (Fig. S1B). To determine the functionality of the zebrafish *mst2* gene, we performed a morpholino (MO)-mediated loss-of-function analysis. Zebrafish embryos treated with *mst2* MO (*mst2* morphants) showed a range of abnormal phenotypes at 52 hours post-fertilization (hpf), from short body length (SL) to abnormal eye pigmentation (AP) and abnormal eye morphology (AM) (Fig. 1A and 1B). RT-PCR analysis confirmed that microinjection of *mst2* MO had effectively prevented correct splicing of the targeted pre-mRNA (Fig. S1C and S1D). These results demonstrate that Mst2 plays a critical role in early zebrafish embryogenesis.

Yap Activity has Important Effects on Early Zebrafish Development

Since Yap is a key effector molecule downstream of the Hippo signaling pathway [12,13], we determined whether overexpression of *yap* induced morphological phenotypes similar to those observed in *mst2* morphants. The amino acid sequence of the Yap protein in the small fish medaka is 85% identical to that of the zebrafish Yap protein and contains the five sites normally phosphorylated by Lats in vertebrate Yap (Fig. S2A). It is now well established that the Hippo pathway regulates Yap's phosphorylation, subcellular localization, and transcriptional coactivator activity, and that this control mechanism is evolutionarily conserved among vertebrates [18]. Some post-translational modifications of Yap, such as its acetylation, are also highly conserved among vertebrates [19]. These observations gave us confidence that medaka Yap (WT) would be functionally comparable with zebrafish Yap (WT) in our experiments. In addition, we generated a constitutively active form of medaka Yap called Yap (5SA) in which the five sites normally targeted by Hippo pathway-dependent phosphorylation were mutated to alanine [20]. Normal zebrafish embryos that were injected with *in vitro*-transcribed medaka *yap (WT)* mRNA were indistinguishable from *EGFP* mRNA-injected control embryos during the first 2 days of development (Fig. 2A). However, by 48 hpf, embryos that had been injected with constitutively active *yap (5SA)* mRNA exhibited the same range of abnormal phenotypes (SL, AP and AM) as seen in the *mst2* morphants (Fig. 2B). These observations indicate that Yap acts downstream of Mst2 to influence early zebrafish development.

The TEAD-binding, WW and Transcription Activation Domains of Yap are Required for Normal Zebrafish Embryogenesis

To define which functional domains of Yap are important for early zebrafish development, we created a series of *yap (5SA)* constructs bearing mutations or deletions inactivating specific Yap domains (Fig. 3). Injection of *yap (5SA)* mRNA led to the same range of developmental defects as presented in Fig. 2B (SL, 19%; AP+SL, 15%; AM+AP+SL, 42%; normal phenotype, 4%; N = 26). Similar results were observed for embryos injected with *yap (5SA)* mRNA missing its SH3-binding domain [*yap (5SA/ΔSH3)*]. In contrast, expression of a *yap (5SA)* mRNA with a defect in the TEAD-binding domain [*yap (5SA/TEAD**)*] reduced the frequency of abnormal phenotypes (AP+SL, 11%; normal phenotype, 68%; N = 19). In addition, the majority of embryos injected with *yap (5SA)* mRNA mutated in both the WW1 and WW2 domains [*yap (5SA/WW1**, *2**)*] exhibited a normal phenotype (AM+AP+SL, 5%; normal phenotype, 89%; N = 19). Finally, almost all embryos injected with *yap (5SA)* mRNA missing its transcription activation domain [*yap (5SA/ΔTA)*] showed a normal phenotype (AM+AP+SL, 3%; normal phenotype, 97%; N = 31). Taken together, these observations demonstrate that overexpression of the TEAD-binding, WW and transcription activation domains of Yap can alter early zebrafish development, and that these domains are therefore critical for normal zebrafish morphogenesis.

Yap Activity Plays a Direct Role in Zebrafish Retinogenesis

Our experiments in Figure 3 showed that injection of *yap (5SA)* mRNA caused abnormal retinal development and body axis malformation. However, it was not clear whether the retinal abnormality was a primary consequence of Yap hyperactivation or a secondary effect caused by the failure in body axis formation. To distinguish between these possibilities, we examined in detail the timing of the emergence of the SL phenotype in *yap (5SA)* mRNA-injected zebrafish embryos. Overexpression of *yap (5SA)* mRNA induced no obvious defects during gastrulation or anterior-posterior axis formation (Fig. S2B), consistent with previous work [21]. After gastrulation, however, the SL phenotype became apparent at 18–21 hpf (Fig. S2C), indicating that increased Yap activity affects the elongation of the body axis during the segmentation period. To minimize the effects of body axis malformation, we generated a *yap (5SA)* construct under the

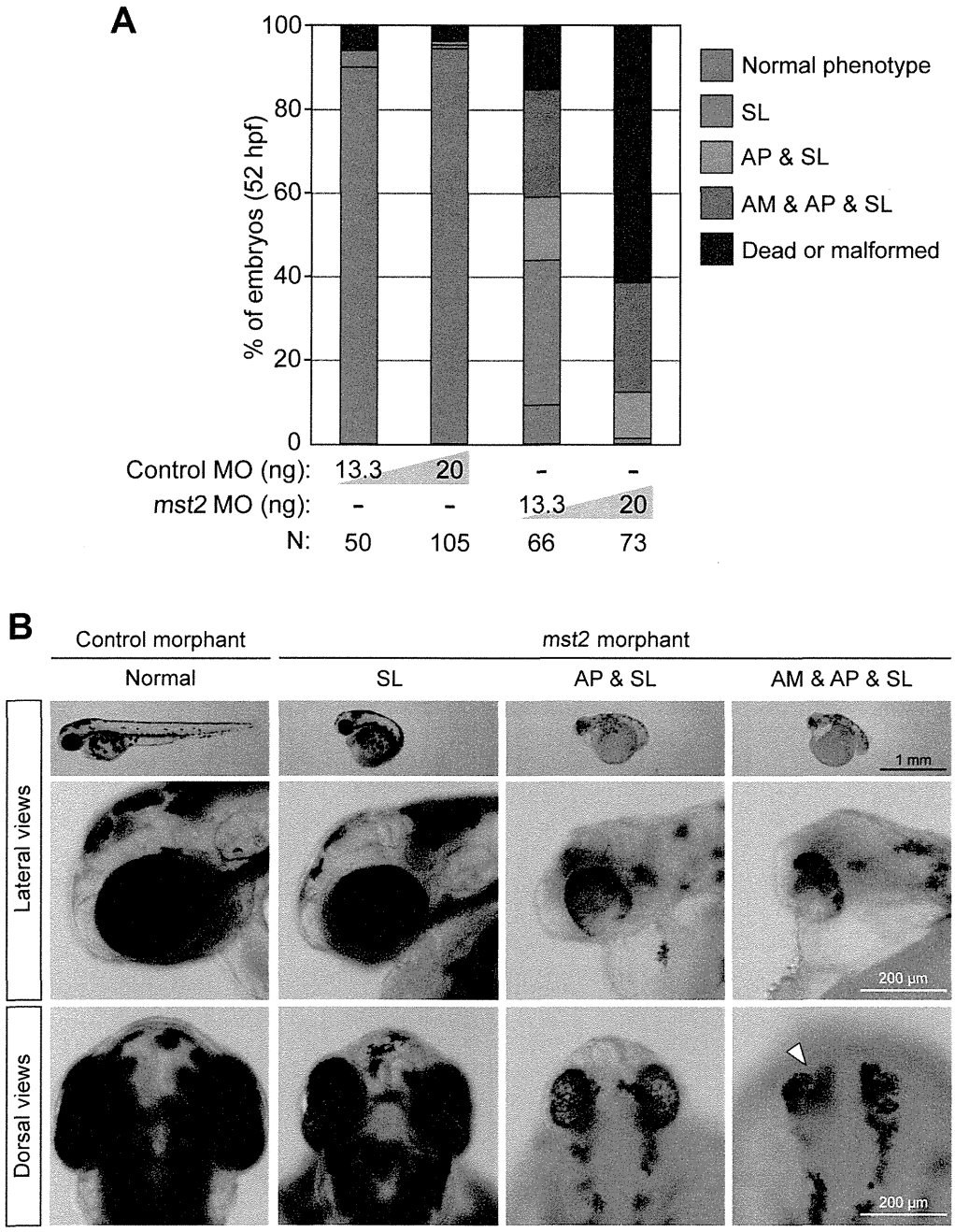

Figure 1. Mst2 is essential for early zebrafish embryogenesis. (A) Early developmental abnormalities of *mst2* morphants. Control or *mst2* morpholino (MO) at the indicated dose was injected into zebrafish embryos and phenotypes were analyzed at 52 hpf. Embryos were classified into five color categories on the basis of their phenotypes: blue, normal embryos; green, short body length (SL); orange, abnormal eye pigmentation (AP) accompanied by SL; red, abnormal eye morphology (AM) plus AP plus SL; and brown, dead or malformed embryos. Results are presented as the percentage of the total number of embryos examined (N). (B) Representative control and *mst2* morphants at 52 hpf. Embryos were injected with control MO (13.3 ng) or *mst2* MO (13.3 ng). Top panels, lateral views of whole embryos. Middle panels, higher magnification images of the head regions of the embryos in the top panels. Bottom panels, dorsal views of the head regions of the embryos in the top panels. (The head is at the top of each panel.) White arrowhead, representative area of AM.
doi:10.1371/journal.pone.0097365.g001

control of the zebrafish heat shock-inducible promoter *hsp70* [*hsp70-EGFP-yap (5SA)*] [22], and induced *yap (5SA)* expression only after 21 hpf (Fig. 4A). Whereas injection alone of *hsp70-EGFP-yap (5SA)* induced no phenotypic alterations, heat shock applied at 21 hpf after injection of *hsp70-EGFP-yap (5SA)* gave rise to abnormal retinal phenotypes (AM and/or AP) (Fig. 4B and 4C). It is noteworthy that, although many embryos also exhibited the SL phenotype (AP+SL, 48%; AM+AP+SL, 9%; N = 23), a sizable proportion showed only an abnormal retinal phenotype (AP, 17%; N = 23). These results support our hypothesis that Yap activity has a direct impact on retinal development.

To achieve retina-specific expression of Yap, we generated a construct containing the upstream region (including the promoter) of the medaka *rx3* gene [*rx-EGFP-yap (5SA)*]. Injection of this

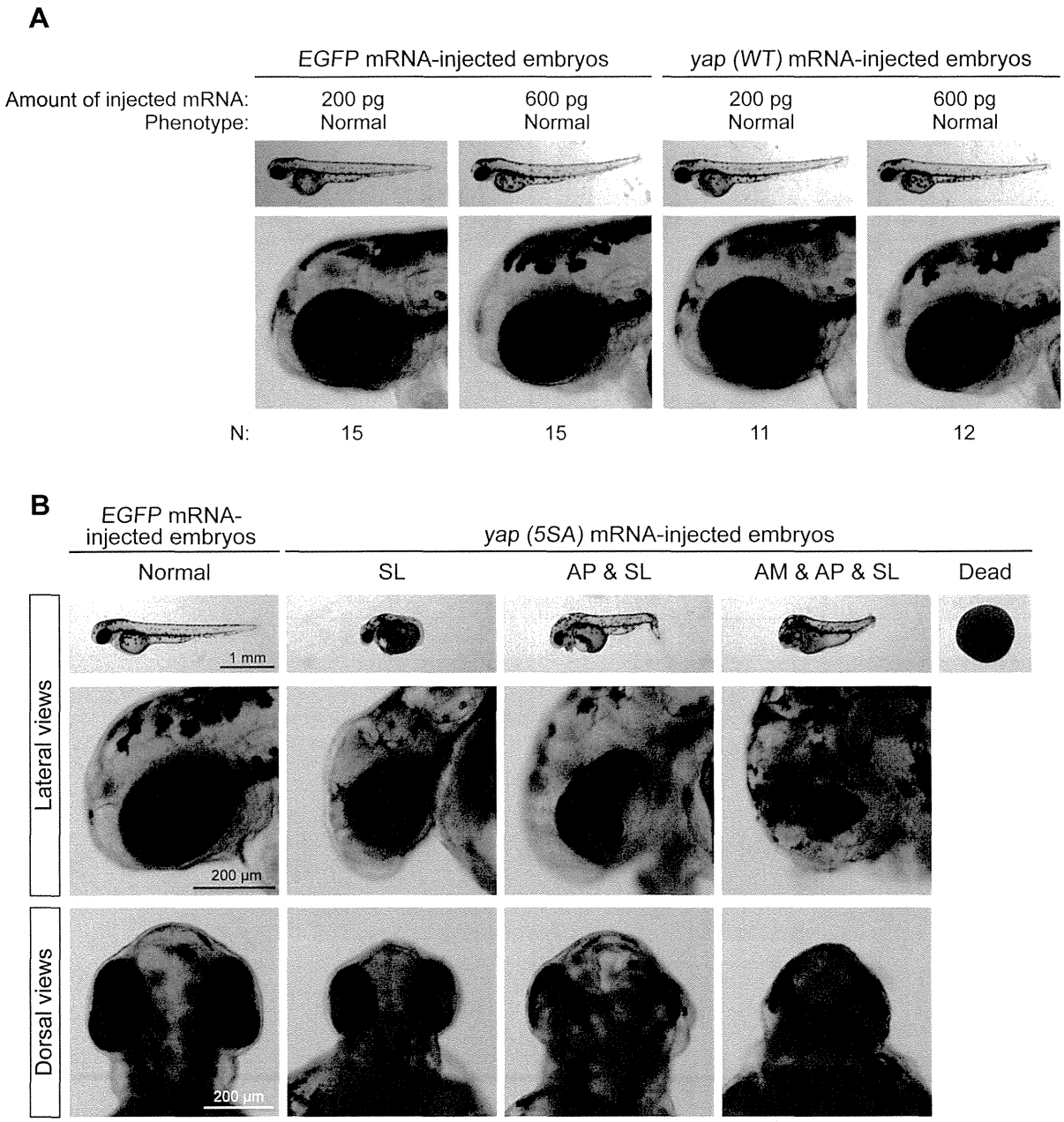

Figure 2. Forced expression of mRNA encoding constitutively active *yap* alters early zebrafish embryogenesis. (A) Representative images of *EGFP* mRNA-injected (control) or *yap (WT)* mRNA-injected zebrafish embryos at 52–54 hpf. Top panels, lateral views of whole embryos. Bottom panels, higher magnification images of the head regions of the embryos in the top panels. N, total number of embryos examined. Embryos injected with either *yap (WT)* mRNA or *EGFP* mRNA had normal phenotypes. (B) Representative images of *EGFP* mRNA-injected (control) or *yap (5SA)* mRNA-injected zebrafish embryos at 48 hpf. Embryos injected with *Yap (5SA)* mRNA (10 pg) showed the same spectrum of abnormal phenotypes as *mst2* morphants. Data are presented as for Fig. 1B.
doi:10.1371/journal.pone.0097365.g002

plasmid into zebrafish embryos resulted in expression of *yap (5SA)* preferentially in the retina (Fig. 5A). Expression of *rx-EGFP-yap (5SA)* gave rise to abnormal eye phenotypes (AM and/or AP) in about 60% of injected embryos (AP, 29%; AM+AP, 31%; N = 45), with no detectable effect on body axis (Fig. 5B and 5C). Conversely, expression of *yap (5SA)* variants mutated in both WW domains [*rx-EGFP-yap (5SA/WW1*, 2*)*] prevented the appearance of abnormal eye phenotypes. These data demonstrate that the two WW domains of Yap mediate activity that directly affects zebrafish retinogenesis.

Retinal Photoreceptor Genes are Downregulated in *yap (5SA)*-expressing Embryos

To conduct a comprehensive survey of transcriptional targets activated downstream of Hippo-Yap signaling during early zebrafish development, we employed a microarray approach and compared genome-wide transcriptomes between *yap (WT)*- and *yap (5SA)*-expressing embryos at three developmental stages (42, 48 and 54 hpf). Gene ontology (GO) analysis revealed that the top two GO categories for genes showing a >4.0-fold decrease in expression in *yap (5SA)*-expressing embryos at each stage were

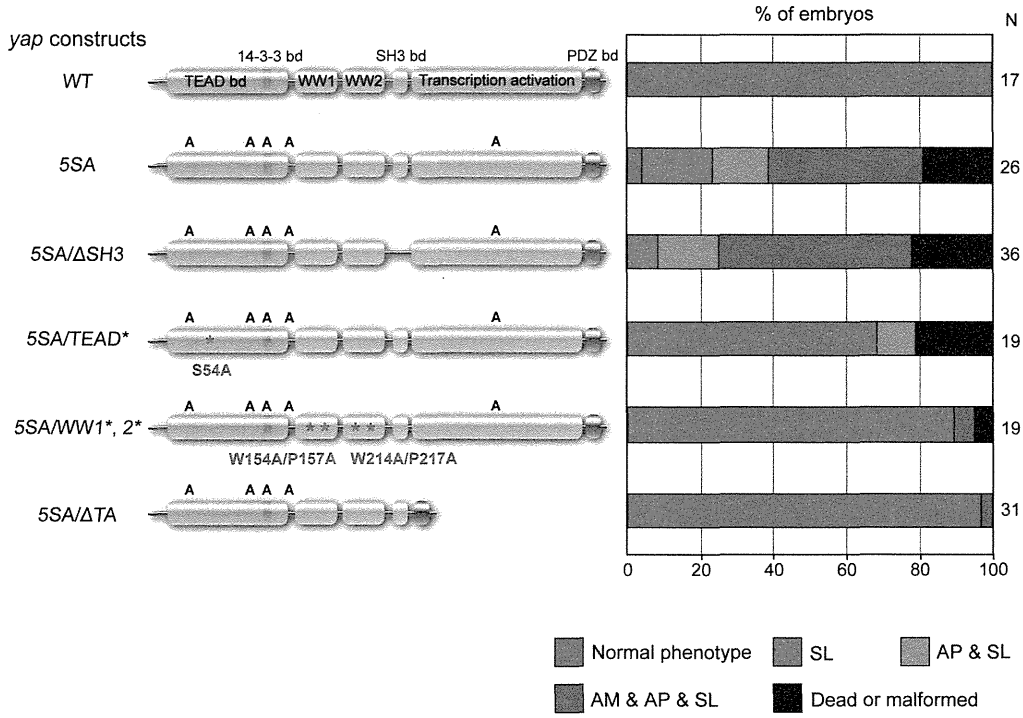

Figure 3. The TEAD-binding, WW and transcription activation domains of Yap contribute to early zebrafish development. Left panel, schematic illustration of constructs of Yap (WT), Yap (5SA), and the indicated variants with deletion (Δ) or mutation (*) of the indicated domains. Specific amino acid alterations are indicated. A, Lats phosphorylation site replaced by an alanine. *In vitro*-synthesized mRNAs (10 pg) derived from these constructs were injected into zebrafish embryos and phenotypes were quantified as shown in the right panel. Color classification is as for Fig. 1A. Results are presented as the percentage of the total number of embryos examined (N).
doi:10.1371/journal.pone.0097365.g003

"phototransduction" and "detection of light stimulus" (Fig. 6A). Strikingly, the retinal photoreceptor gene *rhodopsin* was the gene most downregulated in *yap (5SA)*-expressing embryos compared to *yap (WT)*-expressing embryos (Fig. 6B). This remarkable decrease was 17.0-fold at 42 hpf, an enormous 1,974-fold at 48 hpf, and 449-fold at 54 hpf. Moreover, we found that expression levels of genes encoding photoreceptor TFs such as *crx*, *nr2e3* and *otx5*, which are required for *rhodopsin* transcription [23–25], were greatly reduced in *yap (5SA)*-injected embryos (decreased by 157-, 58.8-, and 29.1-fold, respectively, at 48 hpf) (Fig. 6B). These results indicate that the expression of *yap (5SA)* mRNA affects the transcription of retinal photoreceptor genes.

To confirm Yap's influence on retinal gene expression, we carried out a detailed RT-PCR analysis of mRNA levels in *yap (5SA)*-injected embryos and *mst2* morphants. We found that mRNA levels of *otx2, otx5, crx* and *rhodopsin* were all dramatically downregulated in *yap (5SA)*-injected embryos at 48 hpf compared to *yap (WT)*-injected embryos (Fig. 6C). *Mst2* morphants also displayed decreased mRNA expression of the *otx2*, *crx*, and *rhodopsin* genes (Fig. S3A and S3B). Lastly, because Rx is known to be an upstream transactivator that regulates *otx2* and *rhodopsin* expression in mice and *Xenopus* [9,26], we examined whether expression of the *rx1* and *rx2* genes was reduced in *yap (5SA)*-expressing embryos. Interestingly, levels of *rx1* and *rx2* mRNAs in *yap (5SA)*-injected embryos were comparable to those in *yap (WT)*-injected embryos (Fig. 6C). These results suggest that Yap activity affects zebrafish retinogenesis via transcriptional regulation of photoreceptor genes acting downstream of the *rx* genes.

The Photoreceptor Cell Differentiation Factor Rx1 is a Novel Interacting Partner of Yap

The above microarray and RT-PCR analyses suggested that activated Yap might suppress photoreceptor cell differentiation through interactions with TF(s) acting upstream of *otx*, *crx* and *rhodopsin*. We investigated Rx1 as a candidate TF in this context because zebrafish Rx1 reportedly plays a prominent role in the regulation of retinal photoreceptor differentiation [27]. Intriguingly, we found that zebrafish Rx1 contains an evolutionarily conserved PPXY motif that interacts with Yap's WW domains (Fig. 7A), whereas none of the other three photoreceptor TFs examined (Otx2, Otx5 and Crx) contains a PPXY motif. This observation prompted us to use co-immunoprecipitation analysis to investigate whether Yap and Rx1 could physically interact with each other in cells. Myc-Rx1 was co-expressed with FLAG-Yap (5SA), FLAG-Yap (5SA/WW1*, 2*), or FLAG-Yap (5SA/TEAD*) in HEK293T cells, and cell lysates were subjected to immunoprecipitation with anti-FLAG antibody. We observed that Myc-Rx1 successfully co-immunoprecipitated with either FLAG-Yap (5SA) or FLAG-Yap (5SA/TEAD*) but not with FLAG-Yap (5SA/WW1*, 2*) (Fig. 7B). These results demonstrate that Rx1 can indeed interact with Yap, and that this interaction is mediated by Yap's two WW domains. We also co-expressed FLAG-Yap (5SA) with Myc-Rx1 missing its PPXY motif [Myc-Rx1 (ΔPPXY)] in HEK293T cells and subjected cell lysates to immunoprecipitation with anti-FLAG antibody. Myc-Rx1 (ΔPPXY) did not co-immunoprecipitate with FLAG-Yap (5SA) (Fig. 7C), indicating that the PPXY motif of Rx1 is essential for its interaction with Yap. These data identify the photoreceptor cell differentiation factor Rx1 as a novel interacting partner of Yap, and suggest that

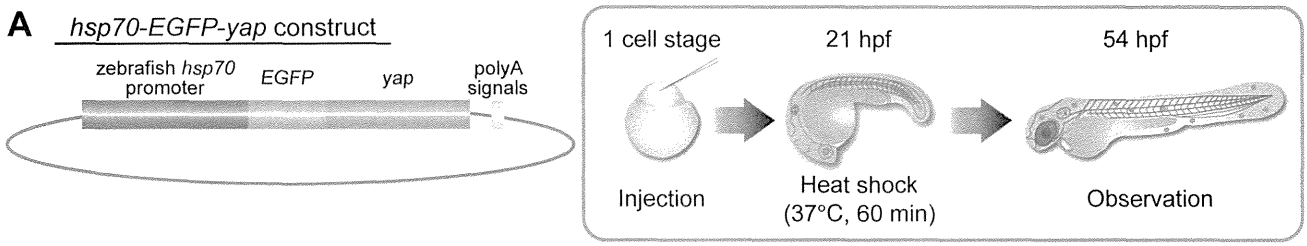
A
hsp70-EGFP-yap construct
zebrafish hsp70 promoter
EGFP
yap
polyA signals
1 cell stage
21 hpf
54 hpf
Injection
Heat shock (37°C, 60 min)
Observation

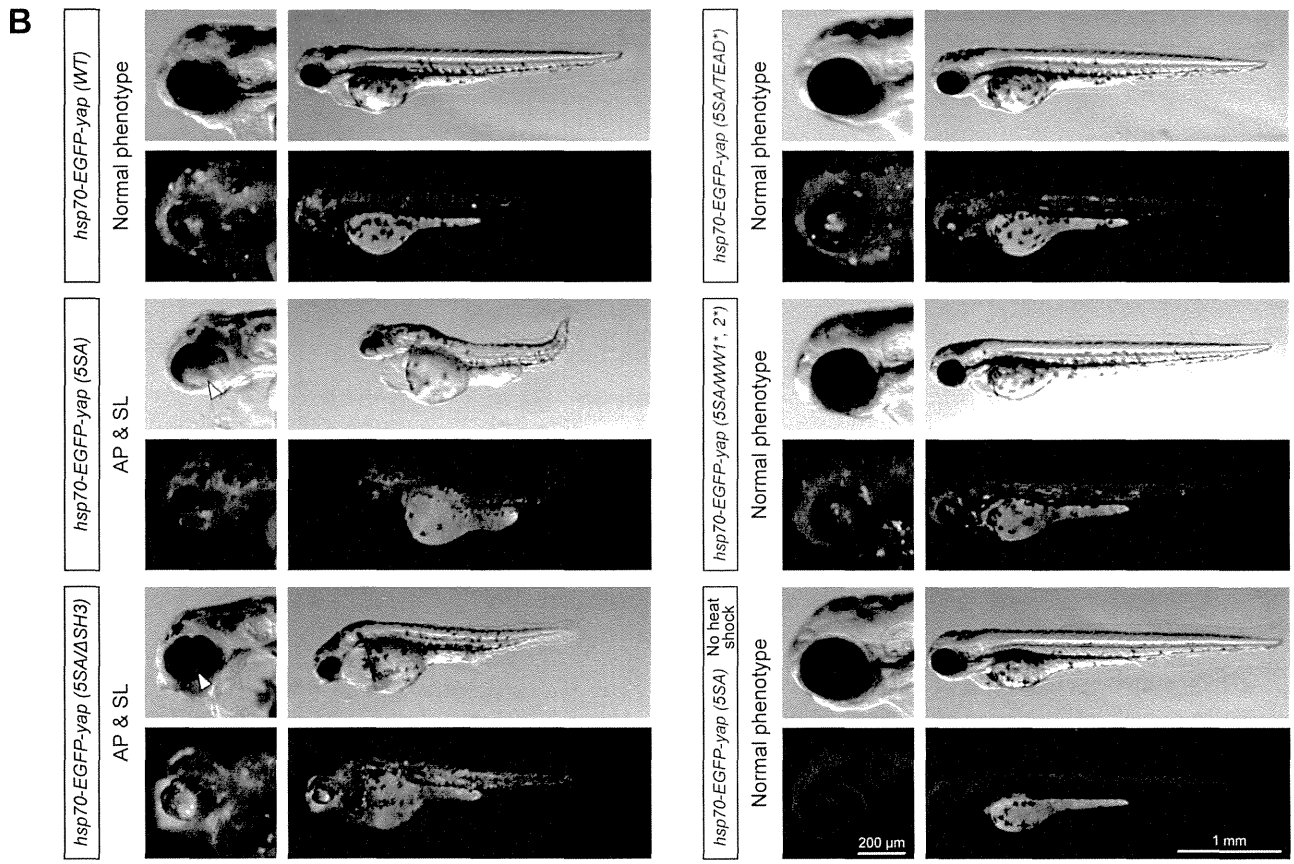
B
hsp70-EGFP-yap (WT)
Normal phenotype
hsp70-EGFP-yap (5SA)
AP & SL
hsp70-EGFP-yap (5SA/ΔSH3)
AP & SL
hsp70-EGFP-yap (5SA/TEAD*)
Normal phenotype
hsp70-EGFP-yap (5SA/WW1*, 2*)
Normal phenotype
hsp70-EGFP-yap (5SA) No heat shock
Normal phenotype
200 µm
1 mm

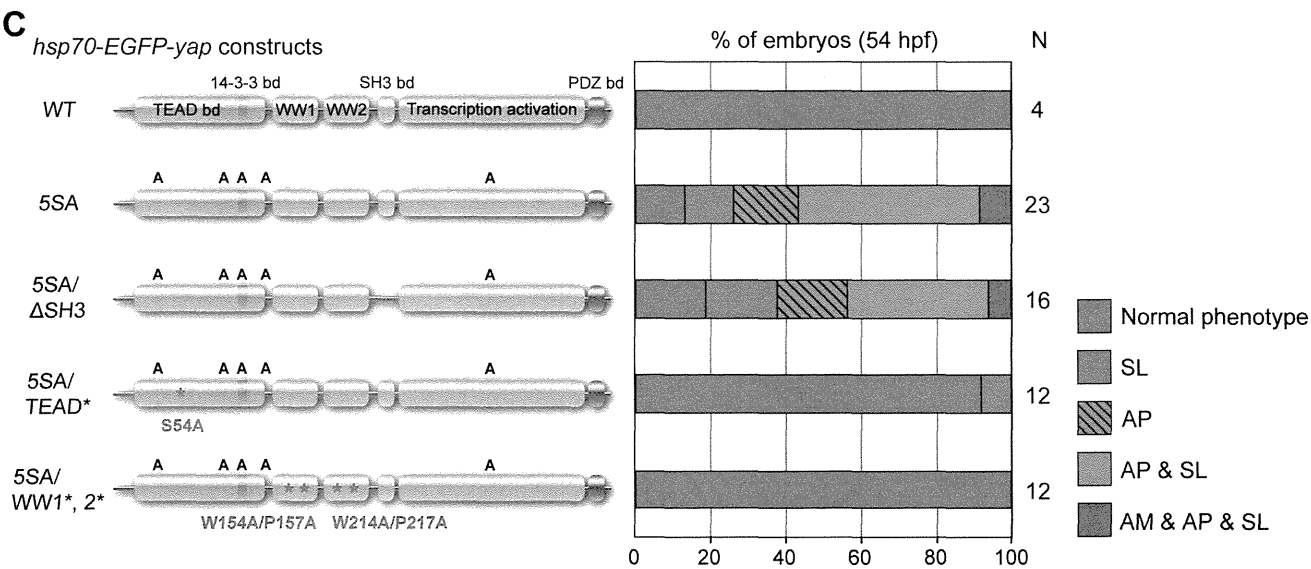
C
hsp70-EGFP-yap constructs
14-3-3 bd
SH3 bd
PDZ bd
WT
TEAD bd
WW1
WW2
Transcription activation
5SA
5SA/ ΔSH3
5SA/ TEAD*
S54A
5SA/ WW1*, 2*
W154A/P157A
W214A/P217A
% of embryos (54 hpf)
N
4
23
16
12
12
0
20
40
60
80
100
Normal phenotype
SL
AP
AP & SL
AM & AP & SL

Figure 4. Yap is directly involved in zebrafish retinogenesis. (A) Schematic illustration of the base *hsp70-EGFP-yap* construct (left panel) and the procedure for the heat shock experiment (right panel). Zebrafish embryos at the one-cell stage were injected with plasmid DNA containing the heat shock promoter constructs indicated in (B). At 21 hpf, injected embryos were immersed in a 37°C water bath for 1 h to apply heat shock and thus induce expression of EGFP-fused Yap. At 54 hpf, EGFP-expressing embryos were isolated and classified on the basis of their phenotypic features. (B) Representative images of the embryos in (A) that were injected with heat shock promoter constructs as indicated on the left side of panels. For each column, top right panels show lateral views of whole embryos, top left panels show higher magnification images of the head regions of the embryos, and bottom panels are fluorescent images of the corresponding top panels. White arrowheads, areas of AP. (C) Quantification of phenotypes of the embryos injected with heat shock promoter constructs in (A, B) as analyzed at 54 hpf. Color classification is as for Fig. 1A except that the phenotype of AP alone is indicated by striped orange shading. Results are presented as the percentage of the total number of embryos examined (N).
doi:10.1371/journal.pone.0097365.g004

Yap may be crucial for coordinating the timing of the terminal differentiation of photoreceptor neurons by suppressing the transcription of the *otx*, *crx* and *rhodopsin* genes.

Discussion

In this study, we examined the role of Hippo-Yap signaling during zebrafish retinogenesis by carrying out an *in vivo* analysis. We demonstrated that knockdown of Mst2 or forced expression of *yap (5SA)* not only disrupts normal embryogenesis as a whole but has specific detrimental effects on retinal pigmentation, eye morphology, and the expression of retinal photoreceptor genes. With respect to embryogenesis, the SL phenotype we observed in our *yap (5SA)* mRNA-injected embryos at 18–21 hpf (Fig. S2C) is similar to that of morphants created in a previous study by knockdown of the zebrafish *yap* gene [17,28]. These latter morphants exhibited a shortened body axis and elevated expression of the somite marker *myoD* during somitogenesis. Our findings thus provide additional evidence that strict control of the activity and localization of Yap is essential for normal somitogenesis during the earliest stages of embryogenesis. Moreover, our data show that Hippo-Yap signaling acts at a later developmental stage as a crucial switch governing retinogenesis.

A key result of our paper is that Yap and the retina-specific TF Rx1 physically interact with each other through Yap's WW domains and Rx1's PPXY motif. Fig. S4 illustrates our proposed model for the bifunctional involvement of Hippo-Yap signaling in determining RPC proliferation versus photoreceptor cell differentiation. When the Hippo pathway is inactive, Yap is activated and associates with TEAD to help drive expression of proliferation-related genes. Simultaneously, activated Yap binds to Rx1 and attenuates its transactivation of photoreceptor genes. The result is the expansion of RPCs and the suppression of photoreceptor cell differentiation. However, when the Hippo pathway is activated by a developmental cue, Yap activation is blocked and the expression of photoreceptor genes is upregulated, promoting the differentiation of mature photoreceptor cells. Thus, in this model, Hippo-Yap signaling is the key molecular mechanism governing the decision of an RPC to self-renew or differentiate.

In *Drosophila*, Hippo is the homolog of mammalian Mst2. In the *Drosophila* eye, Hippo is involved in post-mitotic fate-determining events such as photoreceptor subtype specification [29]. It is conceivable that the primary role of Mst2 in the developing eye is evolutionarily conserved among vertebrate species. In our study of MO-mediated knockdown of zebrafish *mst2*, we showed that this gene is essential for retinal photoreceptor differentiation (Fig. 1A, 1B and S3). In *Xenopus*, Nejigane *et al.* [2013] carried out a loss-of-function analysis of *mst1/2* and found that *mst2* morphants displayed morphogenetic defects, including abnormally small eyes [30]. However, it has been difficult to determine the separate physiological functions of the mammalian *Mst1* and *Mst2* genes during retinal development due to their overlapping tissue expression and functional redundancy. For example, both the *Mst1* KO and *Mst2* KO single null mutant strains are viable and develop normally, suggesting a substantial functional overlap between these two paralogs [31]. Further functional analysis of *Mst1/2* genes in other vertebrates should help to reveal more about the possible evolutionary diversion of Mst1 and Mst2.

Previous studies have implicated Hippo signaling in ocular development [11,16,17,30]. For example, Zhang *et al.* observed that forced expression of Yap in mouse retina prevented proneural bHLH proteins from inducing cell cycle exit, whereas inhibition of Yap decreased RPC proliferation and increased retinal cell differentiation [11]. However, few studies have focused on the molecular mechanism(s) by which Hippo-Yap signaling regulates the differentiation of specific neuronal subtypes such as photoreceptor cells. In our study, we demonstrated that at least three photoreceptor TFs (Otx2, Otx5 and Crx) are activated downstream of Hippo signaling (Fig. 6C and S3). In addition, we discovered that Rx1 is a novel interacting partner of Yap (Fig. 7B), a finding that supplies a missing piece of the puzzle concerning the molecular basis of Hippo-Yap-mediated effects on photoreceptor cell differentiation. In mouse studies, Rx is essential for *otx2* transactivation in the embryonic retina [9]. In *Xenopus* retina, Rx reportedly plays a role in the transcriptional regulation of other retinal photoreceptor genes, such as *rhodopsin* and *red cone opsin* [26]. In zebrafish, Rx1 is required for photoreceptor differentiation [27]. These previous results, together with our present study, support the idea that the timing of activation of both the Rx1-*otx/crx* and Rx1-*rhodopsin* transcriptional cascades is regulated by the Hippo-Yap pathway during zebrafish photoreceptor development.

Our mutational analysis of the Yap (5SA) protein demonstrated that Yap's TEAD-binding, WW, and transcription activation domains all play a pivotal role in the regulation of retinogenesis (Fig. 3). TEAD family members have previously been shown to be critical partners of Yap in regulating neural progenitor cells. For example, Yap functions through TEAD family members to control the proliferation of progenitors in the chicken spinal cord [32]. In the *Xenopus* neural plate, Yap and TEAD1 cooperate to expand neural progenitors and directly regulate *pax3* expression [21]. Our study therefore provides more evidence that the precise regulation of Yap-TEAD interaction is important for maintaining normal neurogenesis. In addition to TEAD family members, PPXY motif-containing TFs, such as ErbB4, p73 and RUNX2, have been shown to interact with Yap via its WW domains [33–35]. For instance, Yap suppresses RUNX2-dependent transcriptional activation of the *osteocalcin* gene promoter [36]. Our study identifies zebrafish Rx1 as a novel photoreceptor differentiation factor, and shows that Rx1's PPXY motif interacts with the WW domains of Yap. This result is consistent with previous observations that many protein interactions associated with Hippo-Yap signaling rely on the binding of a protein's PPXY motif to Yap's WW domains [37–39]. We postulate that Yap functions as a bifunctional transcriptional cofactor by using its TEAD-binding or WW domains; i.e., Yap co-activates the proliferation of RPCs induced by TEAD family members, but also co-represses retinal photoreceptor

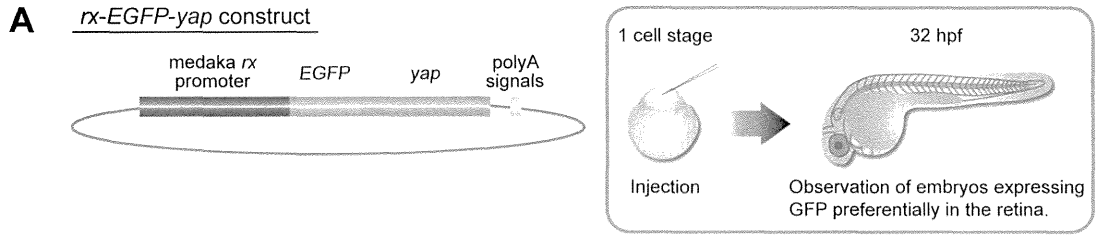
A
rx-EGFP-yap construct
medaka rx promoter
EGFP
yap
polyA signals
1 cell stage
32 hpf
Injection
Observation of embryos expressing GFP preferentially in the retina.

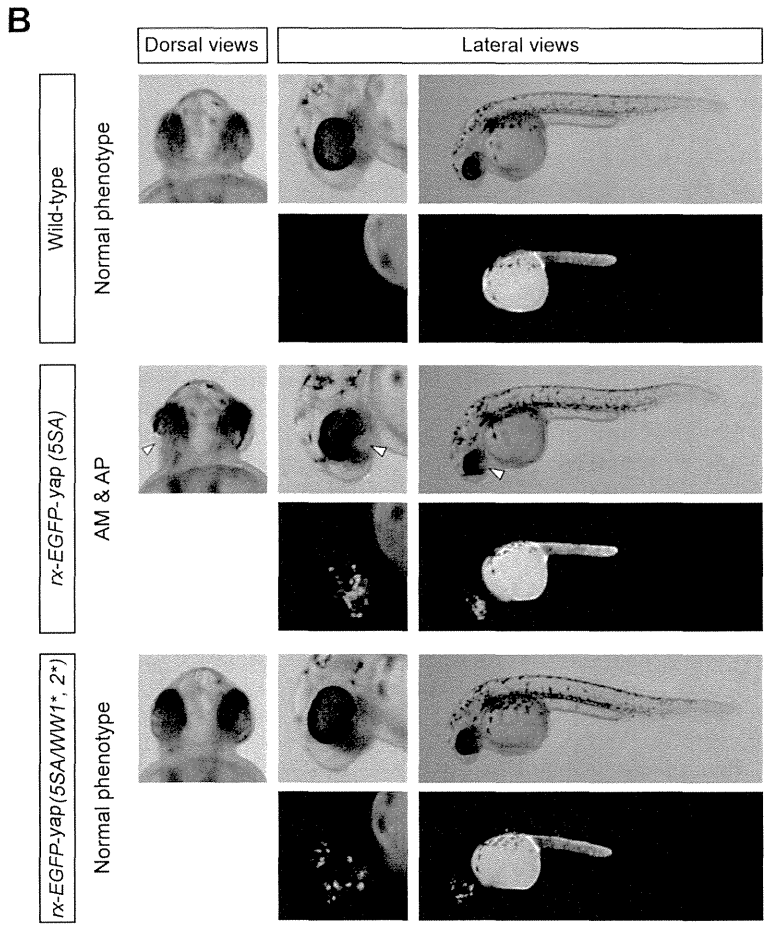
B
Dorsal views
Lateral views
Wild-type
Normal phenotype
rx-EGFP-yap (5SA)
AM & AP
rx-EGFP-yap (5SA/WW1*, 2*)
Normal phenotype

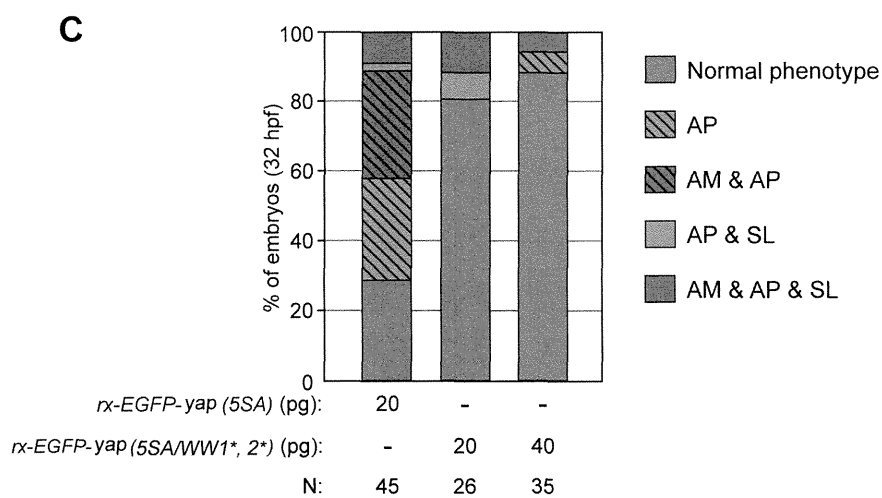
C
100
80
60
40
20
0
% of embryos (32 hpf)
Normal phenotype
AP
AM & AP
AP & SL
AM & AP & SL
rx-EGFP-yap (5SA) (pg): 20 - -
rx-EGFP-yap (5SA/WW1*, 2*) (pg): - 20 40
N: 45 26 35

Figure 5. Retina-specific expression of *yap (5SA)* induces retinogenesis defects without affecting body axis formation. (A) Schematic illustration of the base *rx-EGFP-yap* construct (left panel) and the procedure for the experiment (right panel). Zebrafish embryos at the one-cell stage were injected with plasmid DNA containing the *rx* promoter constructs indicated in (B). (B) Representative dorsal and lateral views of the embryos in (A) that were injected with *rx* promoter constructs as indicated on the left side of panels. Data are presented as for Fig. 4B. White arrowheads, areas of AM plus AP. (C) Quantification of phenotypes of the embryos injected with *rx* promoter constructs in (A, B) as analyzed at 32 hpf. Color classification is as for Fig. 4C except that the phenotype of AM plus AP is indicated by striped red shading. Results are presented as the percentage of the total number of embryos examined (N). Note that expression of *yap (5SA)* variants mutated in both the WW1 and WW2 domains prevented the appearance of abnormal eye phenotypes.
doi:10.1371/journal.pone.0097365.g005

differentiation through interaction of its WW domains with Rx1 (Fig. S4).

It is worth noting that the zebrafish genome contains additional PPXY motif-containing retinal TFs, including ROR members and Nrl (Fig. S5B and S5C); these proteins could also be potential Yap targets. In particular, zebrafish RORα and RORβ possess a PPXY motif that is highly conserved among vertebrate species (Fig. S5B). Furthermore, RORα and RORβ are known to be crucial for photoreceptor cell differentiation because they directly regulate multiple photoreceptor genes [40–42]. Further analyses of TFs expressed in vertebrate photoreceptor tissues should help to evaluate the general role of Yap in photoreceptor cell differentiation.

Yap and its paralogous coactivator TAZ are central nuclear effectors of Hippo signaling and play critical roles in early development [43]. In most vertebrates, Yap occurs both in the Yap1-1 isoform, which has a single WW domain, and in the Yap1-2 isoform, which has tandem WW domains [44]. In contrast, vertebrate TAZ occurs almost exclusively in an isoform with a single WW domain [45]. Recently, a second TAZ isoform was identified in medaka that possesses tandem WW domains like the Yap1-2 isoform [45]. In this study, the affinity between TAZ and PPXY-containing ligands was enhanced by the presence of the additional WW domain, potentially affecting partner protein selection. However, it remains to be determined whether the second TAZ isoform shares binding partners and functional redundancy with the Yap1-2 isoform during early fish development.

Our studies have demonstrated that active Yap can repress retinal photoreceptor cell differentiation, at least in part, by directly blocking the Rx transcriptional machinery. However, the upstream factors that control the timing of Hippo-Yap activation remain unknown. It is possible that the apicobasal polarity protein Crumbs (CRB) is a candidate upstream sensor regulating Yap activity during retinogenesis. Pellissier *et al.* have recently reported that the loss of both CRB1 and CRB2 during early retinogenesis in mice prevents the development of a separate photoreceptor layer and leads to a loss of retinal function that is reminiscent of the abnormalities of humans with Leber Congenital Amaurosis [46]. Pellissier *et al.* also showed that the transcription of *connective tissue growth factor*, a Yap-regulated gene, was reduced in CRB1/CRB2 double KO mice [46], suggesting a critical role for CRB in regulating Yap activity and RPC proliferation during vertebrate retinogenesis. Other cell-extrinsic signals, such as mechanical forces, GPCR ligands, cell density, and serum concentration, have been shown to regulate the Hippo pathway during tissue-specific stem cell differentiation [47]. Understanding exactly how such a variety of microenvironmental signals might coordinate Hippo pathway signaling during RPC/photoreceptor cell fate determination awaits future study.

Materials and Methods

Statement on the Ethical Treatment of Animals

This study was carried out in strict accordance with the recommendations in the ethical guidelines of Tokyo Medical and Dental University. All experimental protocols in this study were approved by the Animal Welfare Committee of Tokyo Medical and Dental University (Permit Number: 2010-212C). All experiments were performed in a manner that minimized pain and discomfort.

Zebrafish Maintenance and Staging

The TL wild type (WT) strain was maintained essentially as described in "The Zebrafish Book" [48]. Embryos were produced by natural matings and staged by standard morphological criteria or by hours or days post-fertilization (hpf or dpf), as described [49].

Phylogenetic Tree

Amino acid sequences of Mst1 and Mst2 of various species were obtained from the Ensembl database. The Ensembl ID numbers of the sequences used were as follows: human MST1 (ENSP00000361892), mouse MST1 (ENSMUSP00000018353), *Xenopus* Mst1 (ENSXETP00000049383), medaka Mst1 (ENSORLP00000024937), pufferfish Mst1 (ENSTNIP00000007894), stickleback Mst1 (ENSGACP00000000023), human MST2 (ENSP00000390500), mouse MST2 (ENSMUSP00000018476), *Xenopus* Mst2 (ENSXETP00000038688), zebrafish Mst2 (ENSDARP00000015367), medaka Mst2 (ENSORLP00000023002), pufferfish Mst2 (ENSTNIP00000012004), stickleback Mst2 (ENSGACP00000004790) and *Drosophila* Hippo (FBpp0085688). A Genescan prediction from the Ensembl database was used to obtain the complete medaka Mst2 sequence. These amino acid sequences were aligned with each other and any positions containing gaps were eliminated. The phylogenetic tree was constructed using the neighbor-joining method and ClustalX software [50]. The reliability of the tree was estimated using the bootstrap method and 10,000 replications.

Antisense Morpholino (MO) against *mst2*

The *mst2* MO (5′-ATGGG CTGTT AAAAC ACAAT GAGGA-3′) was designed to target the splice acceptor site of exon 4 of the zebrafish *mst2* gene (ENSDARG00000011312) and was synthesized by GeneTools, LLC (Philomath, OR). For knockdown, *mst2* MO solution (13.3 or 20 ng) was injected into the yolks of one-cell to four-cell stage zebrafish embryos immediately beneath the cell body. The standard negative control MO (5′-CCTCT TACCT CAGTT ACAAT TTATA-3′) was injected into a control cohort of zebrafish embryos in a similar fashion. Reduction in *mst2* mRNA was confirmed by RT-PCR analysis using the oligonucleotide primer pair 5′-AGCCA TTCAC AAGGA ATCAG G-3′ and 5′-GGTAA GTTGT CCAGC TACTC C-3′.

A

log2 [Yap (5SA)/ Yap (WT)] < -2.0		
Rank	**Gene Ontology**	**Score (p value)**
1	Phototransduction (GO:0007602)	2.97E-59
2	Detection of light stimulus (GO:0009583)	2.98E-57
3	Detection of abiotic stimulus (GO:0009582)	5.10E-56
4	Detection of external stimulus (GO:0009581)	2.39E-49
5	System process (GO:0003008)	3.91E-44

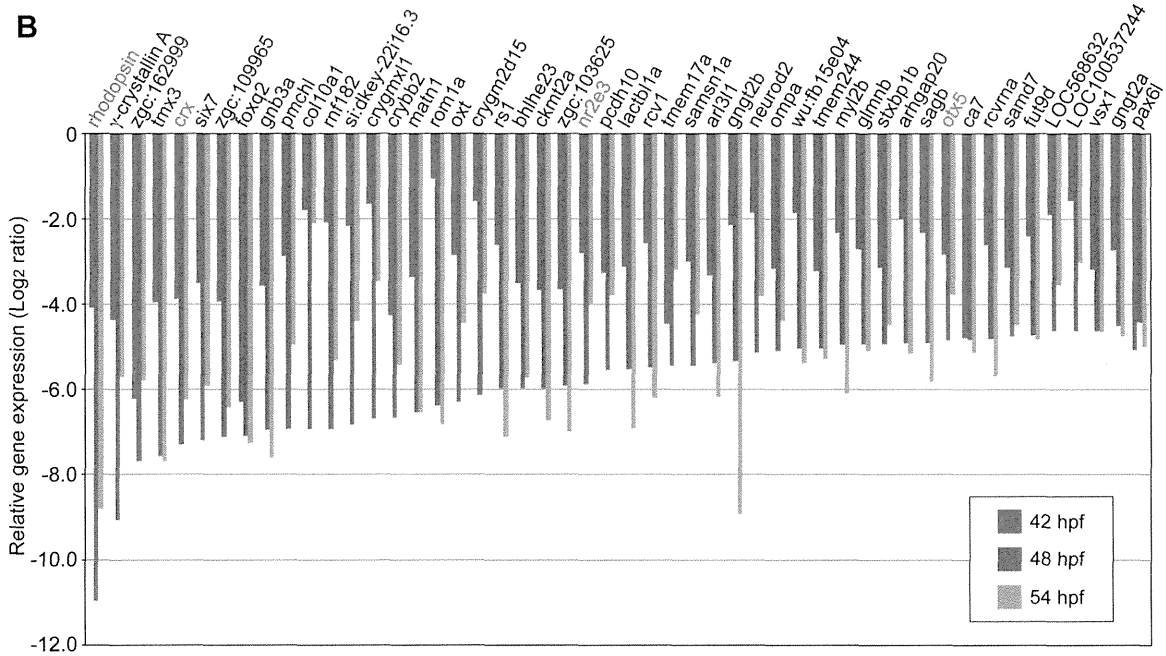

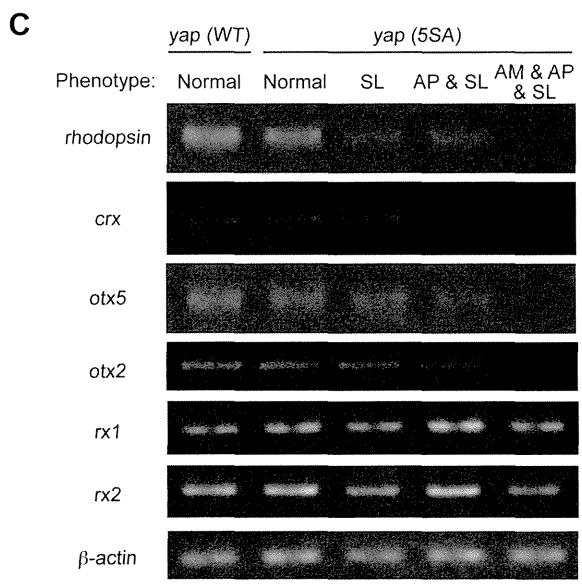

Figure 6. ***Yap (5SA)*** **mRNA-injected embryos exhibit dramatic downregulation of retinal photoreceptor genes.** (A) The top five GO categories for genes downregulated by over 4.0-fold in *yap (5SA)*-expressing embryos at 48 hpf as determined by microarray analysis. (B) A summary of microarray results for the top 50 downregulated genes in the *yap (5SA)*-expressing embryos in (A) compared with *yap (WT)*-expressing embryos at 42, 48 and 54 hpf. The expression levels of genes in the *yap (5SA)*-injected embryos are shown as Log_2 (fold change) values relative to *yap (WT)*-injected embryos. The order of the genes is based on expression levels detected at 48 hpf. Red lettering indicates retinal photoreceptor genes whose expression was severely decreased in *yap (5SA)*-injected embryos. (C) RT-PCR analysis of mRNA expression of the indicated retinal genes in zebrafish embryos injected with *yap (WT)* or *yap (5SA)* mRNA and examined at 48 hpf. β-actin, loading control. *Yap (5SA)*-expressing embryos are grouped by abnormal phenotype, as indicated. Results are representative of two independent experiments.
doi:10.1371/journal.pone.0097365.g006

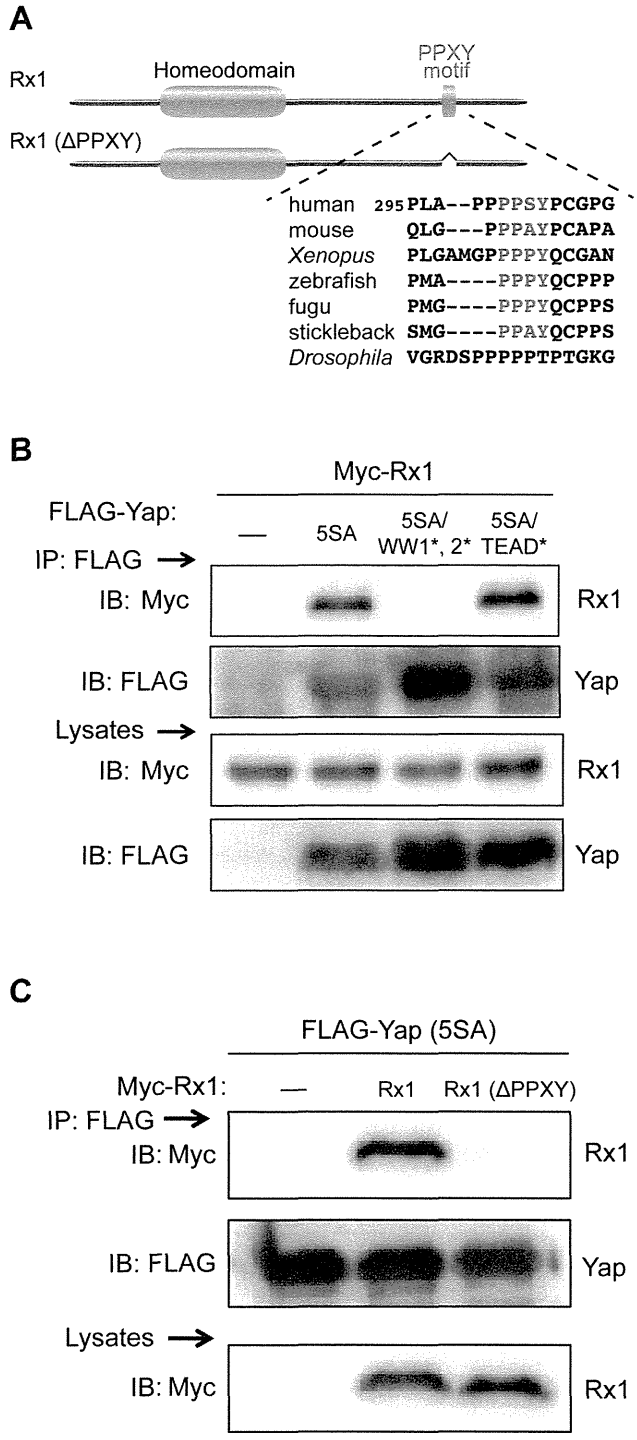

Figure 7. The WW domains of Yap interact with the PPXY motif of Rx1. (A) Schematic illustration of the zebrafish Rx1 and Rx1 (ΔPPXY) constructs. A partial amino acid sequence including the PPXY motif of zebrafish Rx1 was aligned with the sequences of Rx from the indicated species. The PPXY motif (red lettering) is highly conserved among vertebrates. A detailed alignment of Rx family proteins can be found in Fig. S5A. (B) Co-immunoprecipitation analysis of HEK293T cells transiently expressing Myc-Rx1 that were co-transfected with empty vector (–), or vector expressing Yap (5SA), Yap (5SA/WW1*, 2*) or Yap (5SA/TEAD*). Lysates were immunoprecipitated (IP) with anti-FLAG Ab to isolate Yap, followed by Western blotting (WB) with anti-Myc Ab to detect Myc-Rx1 (top), or with anti-FLAG Ab to detect FLAG-Yap (middle). (C) Co-immunoprecipitation analysis of HEK293T cells transiently expressing FLAG-Yap (5SA) that were co-transfected with empty vector (–), or vector expressing Rx1 or Rx1 (ΔPPXY). Lysates were IP'd using anti-FLAG Ab and subjected to WB with anti-Myc Ab to detect Rx1 (top), and with anti-FLAG Ab to detect Yap (middle). Bottom, WB analysis of total cell lysate using anti-Myc Ab to detect Rx1.
doi:10.1371/journal.pone.0097365.g007

Total RNA Extraction and RT-PCR Analysis

Total RNA was isolated from 7–10 zebrafish embryos at 2 dpf using TRIzol reagent according to the manufacturer's protocol (Invitrogen). First-strand cDNA was synthesized from 1 μg total RNA using SuperscriptIII reverse transcriptase (Invitrogen) and oligo-dT primer. Primers used for RT-PCR analysis of mRNA expression in zebrafish extracts were as follows: for *rhodopsin*, 5′-ACAGA GGGAC CGGCA TTCTA CG-3′ and 5′-CAGGC CATGA CCCAG GTGAA G-3′; for *crx*, 5′-AGAGA CGCGG CCGTC CCAAG-3′ and 5′-TCTTC ACGCA TCTTT CCTTC C-3′; for *otx5*, 5′-ACCCT AACAC TCCAC GGAAA C-3′ and 5′-TGCAG TCCAG GCCTG TAAAG-3′; for *otx2*, 5′-ATGAT GTCGT ATCTC AAGCA ACC-3′ and 5′-AGGAA GTGGA ACCAG CATAG CC-3′; for *rx1*, 5′-GATGC CGACA TGTTC TCCAA C-3′ and 5′-CGCCA TGGGC TGCAT GCTTT G-3′; for *rx2*, 5′-GGCTG CCTCT CCACA GAAAG-3′ and 5′-AAACC ACACC TGAAC TCGAA C-3′; for *β-actin*, 5′-CAGCT TCACC ACCAC AGC-3′ and 5′-GTGGA TACCG CAAGA TTCC-3′.

Plasmid Construction

Because our laboratory has been studying the small fish medaka for decades, we took advantage of the availability of medaka *yap (WT)* cDNA and the evolutionary conservation of *yap* sequences among fish species to create plasmids expressing mutated *yap* cDNAs. Our full-length medaka *yap (WT)* cDNA was originally isolated as a homolog of the human *YAP1-2β* isoform [19,44]. We subcloned this cDNA into a modified pCS2+ vector, which positions the FLAG tag at the N-terminus of the insert. The *Yap (5SA)* mutant and its variants with point mutations or deleted domains were generated by the inverse PCR-based method using the primers listed in Table S1. For heat shock experiments, *yap (WT)*, *yap (5SA)* and its variants were cloned into a modified pCS2+ vector in which the CMV promoter was replaced with the zebrafish *hsp70* promoter and the EGFP coding sequence (see Fig. 4A). For retina-specific expression, the zebrafish *hsp70* promoter was replaced with a 4-kb fragment of the medaka *rx3* promoter, which was isolated by PCR using the medaka genome and the primer pair 5′-CCGCC GGCCT CTGAT GTGAT GTTGA CAAA-3′ and 5′-CCCCA TGGTT GTCTA AAAAG GAACT TAAA-3′ (see Fig. 5A) [51]. For co-immunoprecipitation analyses, the PCR-amplified full-length zebrafish *rx1* cDNA was cloned into a pMyc-CMV5 vector (the kind gift of Dr. T. Katada, University of Tokyo), placing the Myc tag at the N-terminus of the insert. The *Rx1* variant in which the PPXY motif was deleted was generated by the inverse PCR-based method using the primers listed in Table S1.

Synthesis of Capped mRNA for Microinjection

Capped sense strand mRNA was synthesized using SP6 RNA polymerase and the mMESSAGE mMACHINE system (Ambion) according to the manufacturer's protocol. RNA injections were performed as described previously [52].

Microarray Analysis

TRIzol reagent was used to extract total RNA at 42, 48 or 54 hpf from whole zebrafish embryos that had been injected with *yap (WT)* or *yap (5SA)* mRNA. RNA quality assurance, cDNA

synthesis, and cRNA labeling and hybridization were carried out by Takara Bio Inc. (Otsu, Japan) using a Zebrafish (V3) Gene Expression Microarray 4X44K, the Low Input Quick Amp Labeling Kit, the Gene Expression Hybridization Kit, and the Gene Expression Wash Buffers Pack (all from Agilent Technologies) according to the manufacturer's protocols. Raw data extraction and analyses were performed using Agilent Feature Extraction software (Agilent Technologies). Gene Ontology analysis was conducted using KeyMolnet software (IMMD Inc., Tokyo, Japan).

Antibodies

Mouse monoclonal anti-FLAG (F1804) and rabbit polyclonal anti-Myc (C3956) antibodies (Abs) were purchased from Sigma–Aldrich Co.

Co-immunoprecipitation Assay

Co-immunoprecipitation assays were performed as previously described [53], with some modifications. HEK293T cells were plated in 10-cm dishes and transfected with the appropriate expression plasmids as described in the Figure Legends. Cells were washed twice with phosphate-buffered saline (PBS) and homogenized in binding buffer [150 mM NaCl, 1 mM EDTA, 0.5% Nonidet P-40, 1 mM EGTA, 5% glycerol, and 20 mM Tris-HCl (pH 7.4)] supplemented with 4 μg/mL aprotinin, 50 mM NaF, and 0.1 mM Na_3VO_4. Extracts were clarified by centrifugation for 10 min at 15,000g, and supernatants were precleared by incubation with 20 μl protein G-agarose beads (GE Healthcare) for 1 h at 4°C. After preclearing, supernatants were incubated with 20 μl anti-FLAG M2-agarose beads (Sigma–Aldrich) overnight at 4°C. The beads were washed three times with binding buffer, boiled in SDS sample buffer, and centrifuged. The supernatants were fractionated by SDS-PAGE and analyzed by Western blotting as described below.

Western Blotting

Immunoprecipitated materials and total cell extracts obtained as described above were fractionated by SDS-PAGE and transferred electrophoretically to PVDF membranes. Membranes were incubated in blocking solution [2% nonfat skim milk in Tris-buffered saline (TBS)] for 1 h at room temperature (RT). Blocked membranes were incubated with anti-FLAG or anti-Myc Ab in 5% BSA/TBS overnight at 4°C. Membranes were washed three times in 0.2% Tween 20 in TBS (TBST), incubated with anti-mouse/rabbit horseradish peroxidase-conjugated Abs in 2% nonfat skim milk in TBS for 1 h followed by three washes in TBST. Proteins were visualized using the SuperSignal West Femto Kit (Pierce) and a ChemiDoc XRS system (Bio-Rad), as described [52].

Supporting Information

Figure S1 Knockdown analysis of the zebrafish *mst2* gene. (A) Alignment of amino acid sequence of zebrafish Mst2 with its human and mouse homologs. Amino acids were aligned using the ClustalX program. Residues are colored according to their physicochemical properties [54]. Gaps have been introduced to optimize alignment. *, critical autophosphorylation site reflecting kinase activation [55]. Black underline, SARAH domain. Arrow, insertion site of the in-frame stop codon in the zebrafish *mst2* morphant. (B) Phylogenetic tree inferred from amino acid sequences of Mst proteins. Statistical significance (%) is shown on each node. Nodes with closed circles represent species divergences, while the node with the open circle represents gene duplication. Scale bar, 0.02 substitutions per site. (C) Top panel, schematic illustration of the target site of the *mst2* MO. Arrows indicate positions of primer pairs used in RT-PCR evaluation of MO efficacy. Bottom panel, partial sequences of native and intron 3-inserted *mst2* mRNAs. The stop codon (in red lettering) occurs in the inserted intron 3 of *mst2* mRNA, resulting in the production of a truncated Mst2 protein. (D) RT-PCR validation of *mst2* MO efficacy. Total RNA was extracted at 52 hpf from embryos injected with control MO (20 ng) or *mst2* MO (13.3 ng) and showing the phenotypes of abnormal eye pigmentation plus short body length (AP & SL), or abnormal eye morphology (AM) plus AP & SL. β-actin, loading control.
(TIF)

Figure S2 Morphological analysis of *yap (5SA)* mRNA-injected zebrafish embryos during the gastrulation and segmentation periods. (A) Alignment of amino acid sequence of medaka Yap with its zebrafish homolog performed as in Fig. S1. *, conserved serine residues phosphorylated by Lats. (B) Representative images of *yap (5SA) mRNA*-injected zebrafish embryos (N = 3) at the indicated developmental stages during gastrulation. Embryos were injected with EGFP mRNA as a control. (C) Representative lateral images of the embryos in (B) examined at the indicated stages during segmentation.
(TIF)

Figure S3 Reduced retinal gene expression in *mst2* morphants. (A) RT-PCR analysis of mRNA levels of the indicated retinal genes in zebrafish embryos injected with control MO or *mst2* MO and examined at 52 hpf. *Mst2* morphants were grouped by abnormal phenotype, as indicated. (B) RT-PCR analysis of *rhodopsin* mRNA expression in the morphants in (A). For A and B, results are representative of two independent trials.
(TIF)

Figure S4 A proposed model for the dual function of Hippo-Yap signaling during retinal progenitor cell proliferation versus photoreceptor cell differentiation. Left panel: When the Hippo pathway is inactive, activated Yap transactivates cell proliferation-related genes via association with TEAD. At the same time, activated Yap represses Rx1-mediated transcription of the *otx, crx* and *rhodopsin* genes, which results in suppression of photoreceptor cell differentiation. Right panel: When the Hippo pathway is active, Yap activation is blocked. TEAD on its own is insufficient to drive cell proliferation-related gene transcription. Without Yap-mediated suppression, Rx1-mediated transcription of *otx, crx* and *rhodopsin* is upregulated, leading to the differentiation of mature photoreceptor cells.
(TIF)

Figure S5 The PPXY motif in retinal transcription factors is highly conserved among vertebrate species. Sequence alignment of C-terminal amino acid residues of the retinal TFs Rx (A), ROR (B) and NRL (C) from the indicated species. Residues are colored according to their physicochemical properties. The red boxes indicate the positions of the PPXY motif. The blue boxes indicate the OAR domain of Rx (transactivation domain), the α-Helix10 domain of ROR, and the leucine zipper of NRL.
(TIF)

Table S1 List of primer sequences for plasmid constructions.
(TIF)

Methods S1 Supporting methods.
(DOC)

Acknowledgments

We thank numerous members of the Nishina laboratories for their helpful discussions and critical comments on the manuscript.

Author Contributions

Conceived and designed the experiments: YA SH MFS HN. Performed the experiments: YA SH MN. Analyzed the data: YA SH MN. Contributed reagents/materials/analysis tools: YA SH MN MFS HN. Wrote the paper: YA MFS HN.

References

1. Livesey FJ, Cepko CL (2001) Vertebrate neural cell-fate determination: lessons from the retina. Nat Rev Neurosci 2: 109–118.
2. Xiang M (2013) Intrinsic control of mammalian retinogenesis. Cell Mol Life Sci 70: 2519–2532.
3. Dowling JE (2012) The retina : an approachable part of the brain. Cambridge, Mass.: Belknap Press of Harvard University Press.: xvi, 355 p. p.
4. Swaroop A, Kim D, Forrest D (2010) Transcriptional regulation of photoreceptor development and homeostasis in the mammalian retina. Nat Rev Neurosci 11: 563–576.
5. Fadool JM, Dowling JE (2008) Zebrafish: a model system for the study of eye genetics. Prog Retin Eye Res 27: 89–110.
6. Stenkamp DL (2011) The rod photoreceptor lineage of teleost fish. Prog Retin Eye Res 30: 395–404.
7. Agathocleous M, Harris WA (2009) From progenitors to differentiated cells in the vertebrate retina. Annu Rev Cell Dev Biol 25: 45–69.
8. Jadhav AP, Mason HA, Cepko CL (2006) Notch 1 inhibits photoreceptor production in the developing mammalian retina. Development 133: 913–923.
9. Muranishi Y, Terada K, Inoue T, Katoh K, Tsujii T, et al. (2011) An essential role for RAX homeoprotein and NOTCH-HES signaling in Otx2 expression in embryonic retinal photoreceptor cell fate determination. J Neurosci 31: 16792–16807.
10. Yaron O, Farhy C, Marquardt T, Applebury M, Ashery-Padan R (2006) Notch1 functions to suppress cone-photoreceptor fate specification in the developing mouse retina. Development 133: 1367–1378.
11. Zhang H, Deo M, Thompson RC, Uhler MD, Turner DL (2012) Negative regulation of Yap during neuronal differentiation. Dev Biol 361: 103–115.
12. Pan D (2010) The hippo signaling pathway in development and cancer. Dev Cell 19: 491–505.
13. Zhao B, Tumaneng K, Guan KL (2011) The Hippo pathway in organ size control, tissue regeneration and stem cell self-renewal. Nat Cell Biol 13: 877–883.
14. Lin YT, Ding JY, Li MY, Yeh TS, Wang TW, et al. (2012) YAP regulates neuronal differentiation through Sonic hedgehog signaling pathway. Exp Cell Res 318: 1877–1888.
15. Hiemer SE, Varelas X (2013) Stem cell regulation by the Hippo pathway. Biochim Biophys Acta 1830: 2323–2334.
16. Lee JH, Kim TS, Yang TH, Koo BK, Oh SP, et al. (2008) A crucial role of WW45 in developing epithelial tissues in the mouse. EMBO J 27: 1231–1242.
17. Jiang Q, Liu D, Gong Y, Wang Y, Sun S, et al. (2009) yap is required for the development of brain, eyes, and neural crest in zebrafish. Biochem Biophys Res Commun 384: 114–119.
18. Hilman D, Gat U (2011) The evolutionary history of YAP and the hippo/YAP pathway. Mol Biol Evol 28: 2403–2417.
19. Hata S, Hirayama J, Kajiho H, Nakagawa K, Hata Y, et al. (2012) A novel acetylation cycle of transcription co-activator Yes-associated protein that is downstream of Hippo pathway is triggered in response to SN2 alkylating agents. J Biol Chem 287: 22089–22098.
20. Zhao B, Wei X, Li W, Udan RS, Yang Q, et al. (2007) Inactivation of YAP oncoprotein by the Hippo pathway is involved in cell contact inhibition and tissue growth control. Genes Dev 21: 2747–2761.
21. Gee ST, Milgram SL, Kramer KL, Conlon FL, Moody SA (2011) Yes-associated protein 65 (YAP) expands neural progenitors and regulates Pax3 expression in the neural plate border zone. PLoS One 6: e20309.
22. Shoji W, Sato-Maeda M (2008) Application of heat shock promoter in transgenic zebrafish. Dev Growth Differ 50: 401–406.
23. Cheng H, Khanna H, Oh EC, Hicks D, Mitton KP, et al. (2004) Photoreceptor-specific nuclear receptor NR2E3 functions as a transcriptional activator in rod photoreceptors. Hum Mol Genet 13: 1563–1575.
24. Furukawa T, Morrow EM, Cepko CL (1997) Crx, a novel otx-like homeobox gene, shows photoreceptor-specific expression and regulates photoreceptor differentiation. Cell 91: 531–541.
25. Whitaker SL, Knox BE (2004) Conserved transcriptional activators of the Xenopus rhodopsin gene. J Biol Chem 279: 49010–49018.
26. Pan Y, Martinez-De Luna RI, Lou CH, Nekkalapudi S, Kelly LE, et al. (2010) Regulation of photoreceptor gene expression by the retinal homeobox (Rx) gene product. Dev Biol 339: 494–506.
27. Nelson SM, Park L, Stenkamp DL (2009) Retinal homeobox 1 is required for retinal neurogenesis and photoreceptor differentiation in embryonic zebrafish. Dev Biol 328: 24–39.
28. Hu J, Sun S, Jiang Q, Sun S, Wang W, et al. (2013) Yes-associated protein (yap) is required for early embryonic development in zebrafish (danio rerio). Int J Biol Sci 9: 267–278.
29. Jukam D, Desplan C (2011) Binary regulation of Hippo pathway by Merlin/NF2, Kibra, Lgl, and Melted specifies and maintains postmitotic neuronal fate. Dev Cell 21: 874–887.
30. Nejigane S, Takahashi S, Haramoto Y, Michiue T, Asashima M (2013) Hippo signaling components, Mst1 and Mst2, act as a switch between self-renewal and differentiation in Xenopus hematopoietic and endothelial progenitors. Int J Dev Biol 57: 407–414.
31. Oh S, Lee D, Kim T, Kim TS, Oh HJ, et al. (2009) Crucial role for Mst1 and Mst2 kinases in early embryonic development of the mouse. Mol Cell Biol 29: 6309–6320.
32. Cao X, Pfaff SL, Gage FH (2008) YAP regulates neural progenitor cell number via the TEA domain transcription factor. Genes Dev 22: 3320–3334.
33. Basu S, Totty NF, Irwin MS, Sudol M, Downward J (2003) Akt phosphorylates the Yes-associated protein, YAP, to induce interaction with 14-3-3 and attenuation of p73-mediated apoptosis. Mol Cell 11: 11–23.
34. Komuro A, Nagai M, Navin NE, Sudol M (2003) WW domain-containing protein YAP associates with ErbB-4 and acts as a co-transcriptional activator for the carboxyl-terminal fragment of ErbB-4 that translocates to the nucleus. J Biol Chem 278: 33334–33341.
35. Yagi R, Chen LF, Shigesada K, Murakami Y, Ito Y (1999) A WW domain-containing yes-associated protein (YAP) is a novel transcriptional co-activator. EMBO J 18: 2551–2562.
36. Zaidi SK, Sullivan AJ, Medina R, Ito Y, van Wijnen AJ, et al. (2004) Tyrosine phosphorylation controls Runx2-mediated subnuclear targeting of YAP to repress transcription. EMBO J 23: 790–799.
37. Bork P, Sudol M (1994) The WW domain: a signalling site in dystrophin? Trends Biochem Sci 19: 531–533.
38. Chen HI, Sudol M (1995) The WW domain of Yes-associated protein binds a proline-rich ligand that differs from the consensus established for Src homology 3-binding modules. Proc Natl Acad Sci U S A 92: 7819–7823.
39. Sudol M, Harvey KF (2010) Modularity in the Hippo signaling pathway. Trends Biochem Sci 35: 627–633.
40. Fujieda H, Bremner R, Mears AJ, Sasaki H (2009) Retinoic acid receptor-related orphan receptor alpha regulates a subset of cone genes during mouse retinal development. J Neurochem 108: 91–101.
41. Jia L, Oh EC, Ng L, Srinivas M, Brooks M, et al. (2009) Retinoid-related orphan nuclear receptor RORbeta is an early-acting factor in rod photoreceptor development. Proc Natl Acad Sci U S A 106: 17534–17539.
42. Srinivas M, Ng L, Liu H, Jia L, Forrest D (2006) Activation of the blue opsin gene in cone photoreceptor development by retinoid-related orphan receptor beta. Mol Endocrinol 20: 1728–1741.
43. Pobbati AV, Hong W (2013) Emerging roles of TEAD transcription factors and its coactivators in cancers. Cancer Biol Ther 14: 390–398.
44. Gaffney CJ, Oka T, Mazack V, Hilman D, Gat U, et al. (2012) Identification, basic characterization and evolutionary analysis of differentially spliced mRNA isoforms of human YAP1 gene. Gene 509: 215–222.
45. Webb C, Upadhyay A, Giuntini F, Eggleston I, Furutani-Seiki M, et al. (2011) Structural features and ligand binding properties of tandem WW domains from YAP and TAZ, nuclear effectors of the Hippo pathway. Biochemistry 50: 3300–3309.
46. Pellissier LP, Alves CH, Quinn PM, Vos RM, Tanimoto N, et al. (2013) Targeted ablation of crb1 and crb2 in retinal progenitor cells mimics leber congenital amaurosis. PLoS Genet 9: e1003976.
47. Yu FX, Guan KL (2013) The Hippo pathway: regulators and regulations. Genes Dev 27: 355–371.
48. Westerfield M (1994) The Zebrafish Book: A Guide for the Laboratory Use of Zebrafish (Branchydanio rerio): Institute of Neuroscience. Eugene, OR: University of Oregon.
49. Kimmel CB, Ballard WW, Kimmel SR, Ullmann B, Schilling TF (1995) Stages of embryonic development of the zebrafish. Dev Dyn 203: 253–310.
50. Saitou N, Nei M (1987) The neighbor-joining method: a new method for reconstructing phylogenetic trees. Mol Biol Evol 4: 406–425.
51. Rembold M, Loosli F, Adams RJ, Wittbrodt J (2006) Individual cell migration serves as the driving force for optic vesicle evagination. Science 313: 1130–1134.
52. Seo J, Asaoka Y, Nagai Y, Hirayama J, Yamasaki T, et al. (2010) Negative regulation of wnt11 expression by Jnk signaling during zebrafish gastrulation. J Cell Biochem 110: 1022–1037.
53. Shimomura T, Miyamura N, Hata S, Miura R, Hirayama J, et al. (2014) The PDZ-binding motif of Yes-associated protein is required for its co-activation of TEAD-mediated CTGF transcription and oncogenic cell transforming activity. Biochem Biophys Res Commun 443: 917–923.
54. Gouy M, Guindon S, Gascuel O (2010) SeaView version 4: A multiplatform graphical user interface for sequence alignment and phylogenetic tree building. Mol Biol Evol 27: 221–224.
55. Praskova M, Khoklatchev A, Ortiz-Vega S, Avruch J (2004) Regulation of the MST1 kinase by autophosphorylation, by the growth inhibitory proteins, RASSF1 and NORE1, and by Ras. Biochem J 381: 453–462.

Biochemical and Biophysical Research Communications 457 (2015) 493–499

Contents lists available at ScienceDirect

Biochemical and Biophysical Research Communications

journal homepage: www.elsevier.com/locate/ybbrc

Extracellular acidification activates ovarian cancer G-protein-coupled receptor 1 and GPR4 homologs of zebra fish

Yuta Mochimaru [a], Morio Azuma [b], Natsuki Oshima [a], Yuta Ichijo [a], Kazuhiro Satou [a], Kouhei Matsuda [b], Yoichi Asaoka [c], Hiroshi Nishina [c], Takashi Nakakura [d], Chihiro Mogi [e], Koichi Sato [e], Fumikazu Okajima [e], Hideaki Tomura [a, *]

[a] Laboratory of Cell Signaling Regulation, Department of Life Sciences, School of Agriculture, Meiji University, Kawasaki 214-8571, Japan
[b] Laboratory of Regulatory Biology, Graduate School of Science and Engineering, University of Toyama, 3190 Gofuku, Toyama 930-8555, Japan
[c] Department of Developmental and Regenerative Biology, Medical Research Institute, Tokyo Medical and Dental University, Tokyo 113-8510, Japan
[d] Department of Anatomy, Graduate School of Medicine, Teikyo University, 2-11-1 Kaga Itabashi-Ku, Tokyo 173-8605, Japan
[e] Laboratory of Signal Transduction, Institute for Molecular and Cellular Regulation, Gunma University, Maebashi 371-8512, Japan

ARTICLE INFO

Article history:
Received 12 December 2014
Available online 7 January 2015

Keywords:
Zebra fish
OGR1
GPR4
Proton sensing

ABSTRACT

Mammalian ovarian G-protein-coupled receptor 1 (OGR1) and GPR4 are identified as a proton-sensing G-protein-coupled receptor coupling to multiple intracellular signaling pathways. In the present study, we examined whether zebra fish OGR1 and GPR4 homologs (zOGR1 and zGPR4) could sense protons and activate the multiple intracellular signaling pathways and, if so, whether the similar positions of histidine residue, which is critical for sensing protons in mammalian OGR and GPR4, also play a role to sense protons and activate the multiple signaling pathways in the zebra fish receptors. We found that extracellular acidic pH stimulated CRE-, SRE-, and NFAT-promoter activities in zOGR1 overexpressed cells and stimulated CRE- and SRE- but not NFAT-promoter activities in zGPR4 overexpressed cells. The substitution of histidine residues at the 12th, 15th, 162th, and 264th positions from the N-terminal of zOGR1 with phenylalanine attenuated the proton-induced SRE-promoter activities. The mutation of the histidine residue at the 78th but not the 84th position from the N-terminal of zGPR4 to phenylalanine attenuated the proton-induced SRE-promoter activities. These results suggest that zOGR1 and zGPR4 are also proton-sensing G-protein-coupled receptors, and the receptor activation mechanisms may be similar to those of the mammalian receptors.

1. Introduction

Mammalian ovarian cancer G-protein-coupled receptor 1 (OGR1) and GPR4 were originally reported to be activated by lysolipids, such as sphingosylphosphorylcholine (SPC) and lysophosphatidylcholine (LPC), which act as ligands [1]; however, the direct binding of the lipids to the receptors has not been proven. On the other hand, Ludwig reported that the human receptors sense extracellular protons and activate intracellular signaling pathways through trimeric G proteins [2]. Thus, human OGR1 stimulation causes phospholipase C (PLC) activation and subsequent intracellular Ca^{2+} ($[Ca^{2+}]_i$) mobilization through $G_{q/11}$ proteins, and human GPR4 stimulates adenylyl cyclase activation through G_s proteins, in response to the extracellular acidification. Later, we showed that human OGR1 is also coupled to G_s/cAMP and G_{13}/Rho signaling pathways [3,4], and GPR4 is coupled to G_{13}/Rho and $G_{q/11}$/PLC signaling pathways [4,5], when the receptors were overexpressed in HEK293T cells. Site mutagenesis studies show that the specific histidine residues at the extracellular surface of the receptors are responsible for proton sensing [2,5].

OGR1 and GPR4 expressions are widely detected in many tissues [1]. The receptor expressions are also reported in vascular endothelial and smooth muscle cells [6–19]. Under an acidic pH condition, OGR1 mediates COX-2, MKP-1, IL-6, CTGF, VCAM-1, and ICAM-1 expressions and PGI_2 production in human vascular smooth muscle and airway smooth muscle cells [15–19]. GPR4 mediates VCAM-1, ICAM-1, COX-2, and a number of inflammatory gene expressions [9,10]. The physiological and pathophysiological

Abbreviations: [1]z, zebra fish (*Danio rerio*); OGR1, ovarian cancer G-protein-coupled receptor 1; GPCR, G-protein-coupled receptor.

* Corresponding author. Fax: +81 44 934 7825.
E-mail address: tomurah@meiji.ac.jp (H. Tomura).

http://dx.doi.org/10.1016/j.bbrc.2014.12.105
0006-291X/

roles of OGR1 and GPR4 are examined using OGR1-and GPR4-deficient mice. However, the molecular mechanism by which the receptors are concerned with the phenotype is largely unknown.

Zebra fish can provide a useful vertebrate model system to elucidate the molecular mechanism of the receptor functions in vivo. The embryo is transparent, and development takes place outside the maternal body. These characteristics make them suitable to use for in vivo imaging. Indeed, zebra fish have been used in especially studies of blood vessel formation [20] and cancer invasion [21].

We found zebra fish OGR1 and GPR4 homologs (zOGR1 and zGPR4) in the genome database; however, their characterizations have not yet been reported. In this study, we characterized the functions of the homologs and focused on their ligand specificity and signaling pathways by expressing them in HEK293T cells. We found that these receptors sense protons like the mammalian receptors and activate multiple signaling pathways.

2. Materials and methods

2.1. Materials

A dual luciferase kit was purchased from Promega (Tokyo, Japan); Fura2 AM from Dojindo (Tokyo, Japan); fatty acid-free BSA from Calbiochem-Novabiochem Co. (San Diego, CA); and Lipofectamine 2000 Reagent from Life Technologies (Tokyo, Japan). The sources of all other reagents were the same as described previously [4,5].

2.2. Preparation of receptor cDNA plasmids and expression

The entire coding regions of zOGR1 (1032 bp, GenBank accession No. XM_001339552), zGPR4 (1122 bp, GenBank accession No. XM_687123), zOGR1-H4F (the 12th, 15th, 162th, and 264th positions of histidine from the N terminus were substituted with phenylalanine), GPR4-H78F (the 78th position of histidine from the N terminus was substituted with phenylalanine), and GPR4-H84F (the 84th position of histidine from the N terminus was substituted with phenylalanine) were synthesized and cloned into a pBo-CMV vector (Takara, Japan) with a Kozak sequence (CCACC) in front of the 1st methionine codon.

The wild-type or the substituted constructs were transfected into HEK293T cells using Lipofectamine 2000 Reagent (Invitrogen, Carlsbad, CA) and plated onto 12 multiplates, as described previously [4].

2.3. Cell cultures

HEK293T cells were provided by the RIKEN BRC through the National Bio-Resource Project of the MEXT, Japan. The cells were cultured in DMEM containing 10% (v/v) FBS (Life Technologies) in a humidified air/CO_2 (19:1) atmosphere.

2.4. Measurement of intracellular calcium

The change in intracellular Ca^{2+} concentration ($[Ca^{2+}]_i$) was measured using a fura-2 method as described previously [22,23]. The changes in the intensities of 540 nm fluorescence obtained by 340 nm and 380 nm excitations were monitored by an FP-8200 spectrofluorometer (JASCO, Tokyo, Japan).

2.5. Dual luciferase reporter assay

cAMP response element (CRE)-, serum response element (SRE)-, or nuclear factor of activated T-cells (NFAT)-driven promoter activity was assayed using the PathDetect Signal Transduction Pathway cis-Reporting Systems (Agilent Technologies, Santa Clara, CA) as described in the previous paper [4].

2.6. Reverse transcriptase (RT) polymerase chain reaction (PCR)

Total RNA was extracted from each 10 embryos or baby fishes at 3, 24, 48, 72, and 96 h post fertilization (hpf). RT-PCR was carried out as follows: preheat at 95 °C for 4 min, then proceed to 34 cycles (OGR1 and GPR4) or 30 cycles (β-actin) at 94 °C for 30 s, 62 °C for 30 s, and 72 °C for 30 s. The forward primers were CGGGACTG-CAACTTCATTGAG for zOGR1, GAAGTGAGACCATGTGCAAC for zGPR4, and GTGATGGACTCTGGTGATGGTGT for zβ-actin. The reverse primers were AGTGGAGTGTGTGTTGAACCTTC for zOGR1, AGAGGTCTGCTATCGAGAGGTTC for zGPR4, and TGAAGCTG-TAGCCTCTCTCGGTC for zβ-actin. The expected size of each product was 204 bp for zOGR1, 201 bp for zGPR4, and 148 bp for zβ-actin.

2.7. Data presentation

All the experiments were performed in duplicate or triplicate. The results of multiple observations are presented as the mean ± SE from more than three different batches of cells unless otherwise stated. Statistical significance was assessed by ANOVA; values were considered significant at $p < 0.05$ (*).

3. Results

3.1. Zebra fish OGR1 and GPR4 homologs sense protons to activate multiple signaling pathways

Transient expression of wild-type zebra fish OGR1 (zOGR1) and GPR4 (zGPR4) homologs in HEK293T cells induced CRE-, SRE-, and NFAT-driven transcriptional activation when the extracellular pH was reduced from 7.6 to 6.3, indicating that these homologs sense protons to activate multiple signaling pathways (Fig. 1A, B). The activated signaling pathways were different between zOGR1 and zGPR4: zOGR1 activates all three (CRE, SRE, and NFAT) pathways. On the other hand, zGPR4 activates CRE and SRE pathways but not the NFAT pathway.

In the previous study [4], we showed that CRE, SRE, and NFAT promoters were activated through the G_s-protein/adenylyl cyclase/cAMP signaling pathway, $G_{12/13}$-protein/Rho signaling pathway, and G_q-protein/phospholipase C–Ca^{2+} signaling pathway in HEK293T cells, respectively. In agreement with this, the $[Ca^{2+}]_i$ was increased, which reflects phospholipase C activation when extracellular pH was reduced from 7.6 to 6.3 in the zOGR1 expressed cells (Fig. 1C). On the other hand, the $[Ca^{2+}]_i$ concentration in the zGPR4 expressed cells was not significantly increased from that in vector-transfected HEK293 cells at pH 6.3 (Fig. 1C). The significant activation of CRE and SRE promoters was observed in the zOGR1 and zGPR4 expressed cells, even at a neutral pH of 7.4 (Fig. 1A, B). Thus, zOGR1 and zGPR4 are stimulated under neutral pH as if the receptors had constitutive activity.

3.2. The similar position of histidine residue in zOGR1 and zGPR4 to that of human receptors is involved in the receptor activation

The histidine residues in the extracellular surface of human OGR1 and GPR4 are crucial for sensing protons [2,5]. The amino acid identity between human and zebra fish OGR1 is 57%, and that between human and zebra fish GPR4 is 73%. The four residues of the five crucial histidine residues (depicted as H in bold type in Fig. 2A) to sense protons in human OGR1 are conserved in zOGR1. To clarify that the histidine residues of zOGR1 play a role to sense protons, we made a construct in which the four histidine residues of the 12th,

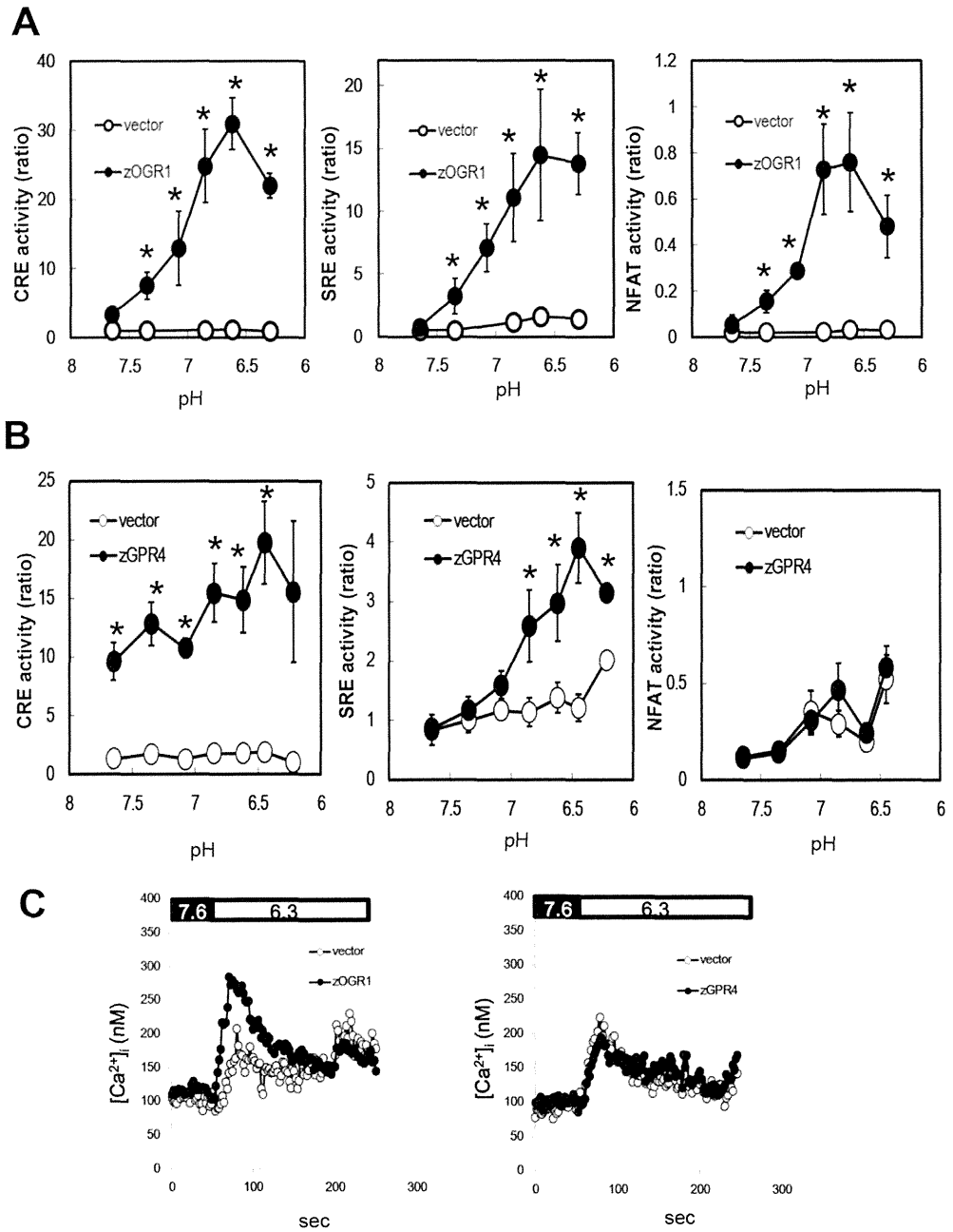

Fig. 1. Extracellular acidic pH-induced CRE-, SRE-, and NFAT-driven transcriptional activation (A, B) and an increment of $[Ca^{2+}]_i$ (C) in zOGR1-and zGPR4-transfected HEK293T cells. In A and B, HEK293T cells were transiently transfected with wild-type zOGR1 and zGPR4 (closed circle) expression plasmids and a pBo-CMV vector (open circle) together with pRL-TK and pCRE-, pSRE-, or pNFAT-luc. The cells were incubated for 6 h at the indicated pH to measure CRE-, SRE-, and NFAT-promoter activities. See "Materials and methods" for more detail. Results are means ± SE. The asterisk (*) indicates that the effects of zOGR1 and zGPR4 were significant under the indicated pH. In C, the cells were harvested from the dishes, and $[Ca^{2+}]_i$ was measured. The typical trace of $[Ca^{2+}]_i$ change by acidic pH (pH 6.3) was shown in the vector-(open circle), zOGR1-, and zGPR4-(closed circle) transfected cells. Two other experiments yielded similar results.

15th, 162th, and 264th positions from the N terminus of zOGR1 were substituted with phenylalanine (H4F) and examined the SRE-promoter activities upon reducing extracellular pH from 7.6 to 6.3. As shown in the left panel of Fig. 2C, the mutant showed little activity. Thus, the histidine residues, which are crucial for sensing protons in human OGR1, are conserved in zOGR1. Next we examined whether the similar position of histidine residue is responsible for proton sensing. Based on the result of human GPR4 [5], the histidine residue of the 78th amino acid from the N terminus of zGPR4 is supposed to play a role to sense protons. On the other hand, the histidine residue of the 84th amino acid may be not to play that role. We made two different mutants in which the histidine residues at the 78th and 84th positions were substituted with phenylalanine (H78F and H84F, respectively) and examined their activity. As expected, the H78F mutant showed reduced SRE-promoter activity compared with the activity of wild-type zGPR4; however, the activity of the H84F mutant was comparable to the activity of the wild type (Fig. 2C, right panel). This suggests that the histidine position for proton sensing is conserved between the human and zebra fish receptors.

A

```
H.sapiens       MGNITADNSSMSCTIDHTIHQTLAPVVYVTVLVVGFPANCLSLYFGYLQIKARNELGVYL 60
D.rerio         -----MSEEQINCTINHDIHQYLFSVAYLLVLLVGLPANAYSLYHAWLQLKARNELGVYL 55

H.sapiens       CNLTVADLFYICSLPFWLQYVLQHDNWSHGDLSCQVCGILLYENIYISVGFLCCISVDRY 120
D.rerio         LNLTISDLLYLGSLPLWLQYIFQGDNWSGSEWLCQLCGFLLYENIYVSIGFLCCISIDRY 115

H.sapiens       LAVAHPFRFHQFRTLKAAVGVSVVIWAKELLTSIYFLMHEEVIEDENQHRVCFEHYPIQA 180
D.rerio         LAVVYPFRFSAFRTVRAATLVSTVVWLKELAVGVVFFLHKELSRDKHNQSVCFEHYPMKT 175

H.sapiens       WQRAINYYRFLVGFLFPICLLLASYQGILRAVRRSHGTQKSRKDQIQRLVLSTVVIFLAC 240
D.rerio         WEYQINYYRFYIGFLFPLGILSVSYFRVLRAVGKSAGTQTSQKIRIKYLVTSTIVIFLVC 235

H.sapiens       FLPYHVLLLVRSVWEASCDFAKGVFNAYHFSLLLTSFNCVADPVLYCFVSETTHRDLARL 300
D.rerio         FSPYHIFLLVRTIFERDCNFIESIFNYYHFSLLLTSFNCVADPALYCFISESAQKGIQKA 295

H.sapiens       RGACLAFLTCSRTGRAREAYPLGAPEASGKSGAQGEEPELLTKLHPAFQTPNSPGSGGFP 360
D.rerio         HDACTRVFCCCSKSHGRFNTHSTELAVTNDNVTGTSVVTLLQQIKTEV------------ 343

H.sapiens       TGRLA 365
D.rerio         -----
```

B

```
H.sapiens       ---------MGNHTWEGCHVDSRVDHLFPPSLYIFVIGVGLPTNCLALWAAYRQVQQRNE 51
D.rerio         MASLRGSETMCNITTS-CNVDSNIDQFFQPTLYIIVIVLGFPTNCMALWAAYMQVKQKNE 59

H.sapiens       LGVYLMNLSIADLLYICTLPLWVDYFLHHDNWIHGPGSCKLFGFIFYTNIYISIAFLCCI 111
D.rerio         LGIYLMNLSIADLLYITTLPLWIDYFVHHDNWIHGQVSCKLFGFIFYTNIYVSIAFLCCI 119
                                          78    84

H.sapiens       SVDRYLAVAHPLRFARLRRVKTAVAVSSVVWATELGANSAPLFHDELFRDRYNHTFCFEK 171
D.rerio         SVDRYLAVAHPLKFAKVRRVKTALLVSAIVWLTEIVANSAPLFHDELFQDRFNHTFCFEK 179

H.sapiens       FPMEGWVAWMNLYRVFVGFLFPWALMLLSYRGILRAVRGSVSTERQEKAKIKRLALSLIA 231
D.rerio         YPMEPWVAGMNLYRTFLGFLAPWGIMLAAYRGILRAVRGNVSTERQEKAKIKRLALSLIL 239

H.sapiens       IVLVCFAPYHVLLLSRSAIYLGRPWDCGFEERVFSAYHSSLAFTSLNCVADPILYCLVNE 291
D.rerio         IVLLCFAPYHVLLLWRSVLFLINPCDCGGEENLFGAYHVTLALTSLNCVADPILYCFVNE 299

H.sapiens       GARSDVAKALHNLLRFLASDK-PQEMANASLTLETPLTSKR-NSTAKAMTGSWAATPPSQ 349
D.rerio         GARHDVGRALATLLGLFQRGKSPETLMGASITVETPLAVKKPDFYSEVKTNAYKNDIEVL 359

H.sapiens       GDQ-VQLKMLPPAQ 362
D.rerio         KDECLQMTILSVKK 373
```

C

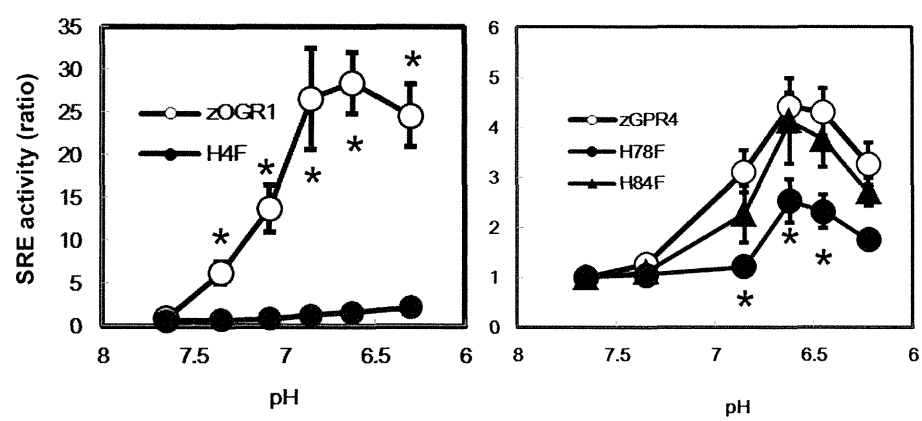

Fig. 2. Amino acid sequence alignment between OGR1 (A) and GPR4 (B) of humans (H.sapiens) and zebra fish (*D. rerio*) and the effects of the substitution of histidine with phenylalanine in zOGR1 and zGPR4 on proton-induced SRE-promoter activity (C). The histidine (H), which is concerned with the proton sensing of human OGR1 and GPR4, is depicted in bold type. All the corresponding histidines of zOGR1 were substituted with phenylalanine (H4F). The number in B indicates the mutant, whose histidine was substituted with phenylalanine in zGPR4 (H78F or H84F). HEK293T cells were transiently transfected with wild-type zOGR1, zGPR4 together with pRL-TK, and pSRE-luc. The cells were incubated for 6 h at the indicated pH to measure SRE-promoter activity. Results are means ± SE. The asterisk (*) indicates that the activities of H4F and H78F were significantly different from those of the wild-type receptors under the indicated pH.

3.3. LPC and SPC do not seem to mediate SRE activation in the zOGR1 and zGPR4 overexpressed cells

LPC and SPC modulate the mammalian OGR1-and GPR4-mediated cell responses [3,6,11,24–28]. We next examined whether these lysolipids modulate the zOGR1-and/or GPR4-mediated SRE-promoter activation. As shown in the right panels of Fig. 3A and B, SPC at 10 μM induced SRE-promoter activation; however, similar activation was also detected in the vector-transfected cells. Thus, SPC does not modulate zOGR1-and zGPR4-mediated SRE-reporter activation. LPC at 10 μM did not stimulate SRE-promoter activation (Fig. 3A and B, left panels).

3.4. zOGR1 and zGPR4 were expressed in zebra fish

We finally examined the gene expression of zOGR1 and zGPR4 at different developmental stages of zebra fish embryogenesis (Fig. 4). Both receptors were expressed in zebra fish; however, the expression pattern was different, i.e., the transcript of zOGR1 was detected in the stages from 24 to 96 hpf. On the other hand, the transcript of zGPR4 was present in all the analyzed stages from 3 to 96 hpf.

4. Discussion

In the present study, we show for the first time that OGR1 and GPR4 homologs of zebra fish sensed protons and activated the multiple signaling pathways (Fig. 1A and B). Thus, zOGR1 and zGPR4 are proton-sensing GPCRs, as are human OGR1 and GPR4; however, the NFAT-reporter activation profile was different between zebra fish and human GPR4. In the previous study [4,5], extracellular acidification induced NFAT-driven transcriptional activity of human GPR4; however, the transcriptional activity of zGPR4 was not attenuated at any pH tested (Fig. 1B). It may be due to a difference of coupling efficiency to human $G_{q/11}$ between human and zebra fish GPR4. It should be investigated in the future. The high CRE-reporter activation of zGPR4 was detected even at pH 7.6 and was further enhanced by extracellular acidification (Fig. 1B). The increment of cAMP accumulation is also detected even at pH 7.6 in the original report [2]. This is not due to the effect of overexpression of GPR4. The high cAMP accumulation at pH 7.8 is reported in the kidney cells [29].

The specific histidine residues of human OGR1 and GPR4 play a crucial role in sensing extracellular protons [2,5,30]. Five histidine residues (depicted as H in bold type in Fig. 2A) are responsible for sensing and activating the signaling pathways in human OGR1 [14,31]. Four of the five corresponding positions of histidine residues are conserved in zOGR1 (Fig. 2A). In this study, the mutant that was substituted in these four histidine residues with phenylalanine failed to stimulate the SRE-reporter (Fig. 2C, left panel). This result suggests that the activation mechanisms are similar between human and zebra fish OGR1. We confirmed the similarity of the receptor activation between human and zebra fish using the zGPR4 mutants (Fig. 2B). As shown in Fig. 2C, the mutant of the 78th but not of 84th position attenuated acidic pH-induced SRE-reporter activation. This result is the same as the result of human GPR4 [5]. The similarity between the human and zebra fish receptors

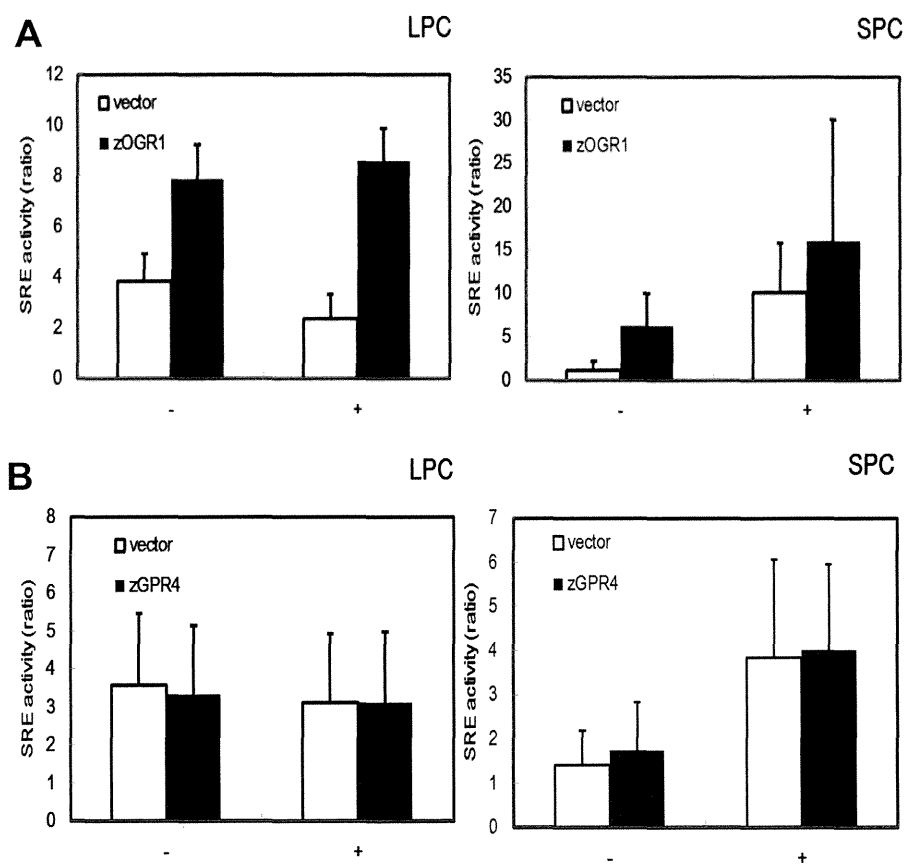

Fig. 3. Effect of SPC and LPC on SRE-promoter activity in zOGR1 (A) and zGPR4 (B) overexpressed HEK292T cells. HEK293T cells were transiently transfected with wild-type zOGR1 and with zGPR4 together with pRL-TK and pSRE-luc. The cells were incubated for 6 h in the presence (+) or absence (−) of 10 μM LPC or 10 μM SPC to measure SRE-promoter activity. Results are means ± SE of six determinations from two separate experiments.

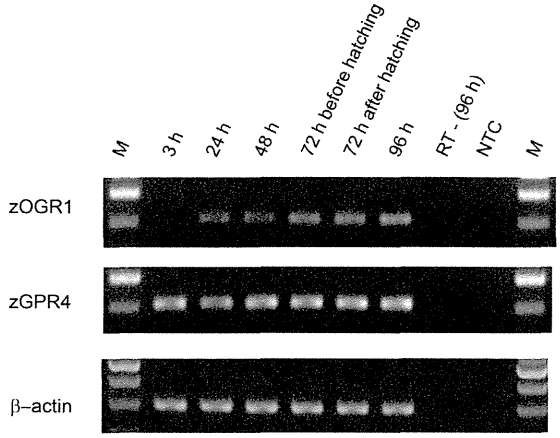

Fig. 4. Expression pattern of zOGR1 or zGPR4 transcripts during zebra fish embryogenesis. RT-PCR reactions were performed at different stages of embryogenesis. The developmental stage was depicted as hours post fertilization (h) on top of the figure. β-actin was used as a control of RT-PCR. RT-indicates a negative PCR control reaction without reverse transcriptase reaction. NTC also indicates a negative control reaction without RNA. M indicates a 100 bp molecular weight marker. The expected size of zOGR1 is 204 bp, and that of zGPR4 is 201 bp.

suggests that we can use zebra fish for the screening of chemical compounds that will have agonist and/or antagonist activity with human OGR1 and GPR4.

Human OGR1 and GPR4 were originally reported as the receptors for SPC and LPC; however, the report was retracted. In this study, we examined the possibility of whether these lysolipids stimulate the zOGR1-and zGPR4-mediated pathways. As shown in Fig. 3, LPC did not stimulate the zOGR1-or zGPR4-induced reporter activity. On the other hand, SPC stimulated SRE-promoter activation; however, similar activation was also detected in vector-transfected cells. This zOGR1-and zGPR4-independent SPC action may be partly mediated by endogeneous S1P receptors [4].

zOGR1 and zGPR4 were expressed in various developmental stages of zebra fish (Fig. 4). These receptors may play physiological and pathophysiological common roles in vertebrates. The physiological and pathophysiological roles of OGR1 and GPR4 have been examined using OGR1-and GPR4-deficient mice. OGR1-deficient mice show tumor growth inhibition [32], enhanced proton extrusion in the proximal tube of the kidney [14], and decreased insulin secretion from the islet [33]. GPR4-deficient mice show vascular abnormality [12], reduced angiogenesis and tumor growth [34], decreased acid secretion from the kidney [29], and improved glucose tolerance and insulin sensitivity [35]. However, the molecular mechanism by which the receptors are concerned with the phenotype is largely unknown.

Zebra fish have been extensively used for in vivo imaging, especially in the studies of blood vessel formation [20] and cancer invasion [21]. Since OGR1-and GPR4-deficient mice show the receptors' effect on tumor growth and vascular formation, as described above, zebra fish studies will provide useful information for the physiological and pathophysiological roles of OGR1 and GPR4 in the future.

Disclosure statement

The authors have declared no conflicts of interest.

Acknowledgments

This work was supported by Grants-in-Aid (C) for Scientific Research from the Japan Society for the Promotion of Science Grant Number 24580436 and the MEXT-Supported Program for the Strategic Research Foundation at Private Universities, 2014–2018.

References

[1] Y. Xu, Sphingosylphosphorylcholine and lysophosphatidylcholine: G protein-coupled receptors and receptor-mediated signal transduction, Biochim. Biophys. Acta 1582 (2002) 81–88.
[2] M.G. Ludwig, M. Vanek, D. Guerini, J.A. Gasser, C.E. Jones, U. Junker, H. Hofstetter, R.M. Wolf, K. Seuwen, Proton-sensing G-protein-coupled receptors, Nature 425 (2003) 93–98.
[3] C. Mogi, H. Tomura, M. Tobo, J.Q. Wang, A. Damirin, J. Kon, M. Komachi, K. Hashimoto, K. Sato, F. Okajima, Sphingosylphosphorylcholine antagonizes proton-sensing ovarian cancer G-protein-coupled receptor 1 (OGR1)-mediated inositol phosphate production and cAMP accumulation, J. Pharmacol. Sci. 99 (2005) 160–167.
[4] M. Tobo, H. Tomura, C. Mogi, J.Q. Wang, J.P. Liu, M. Komachi, A. Damirin, T. Kimura, N. Murata, H. Kurose, K. Sato, F. Okajima, Previously postulated "ligand-independent" signaling of GPR4 is mediated through proton-sensing mechanisms, Cell. Signal. 19 (2007) 1745–1753.
[5] J.P. Liu, T. Nakakura, H. Tomura, M. Tobo, C. Mogi, J.Q. Wang, X.D. He, M. Takano, A. Damirin, M. Komachi, K. Sato, F. Okajima, Each one of certain histidine residues in G-protein-coupled receptor GPR4 is critical for extracellular proton-induced stimulation of multiple G-protein-signaling pathways, Pharmacol. Res. 61 (2010) 499–505.
[6] K.S. Kim, J. Ren, Y. Jiang, Q. Ebrahem, R. Tipps, K. Cristina, Y.J. Xiao, J. Qiao, K.L. Taylor, H. Lum, B. Anand-Apte, Y. Xu, GPR4 plays a critical role in endothelial cell function and mediates the effects of sphingosylphosphorylcholine, Faseb J. 19 (2005) 819–821.
[7] B. Dong, H. Zhou, C. Han, J. Yao, L. Xu, M. Zhang, Y. Fu, Q. Xia, Ischemia/Reperfusion-induced CHOP expression promotes apoptosis and impairs renal function recovery: the role of acidosis and GPR4, PLoS One 9 (2014) e110944.
[8] J. Ren, W. Jin, Y.E. Gao, Y. Zhang, X. Zhang, D. Zhao, H. Ma, Z. Li, J. Wang, L. Xiao, R. Liu, Y. Chen, J. Qian, L. Niu, H. Wei, Y. Liu, Relations between GPR4 expression, microvascular density (MVD) and clinical pathological characteristics of patients with epithelial ovarian carcinoma (EOC), Curr. Pharm. Des. 20 (2014) 1904–1916.
[9] L. Dong, Z. Li, N.R. Leffler, A.S. Asch, J.T. Chi, L.V. Yang, Acidosis activation of the proton-sensing GPR4 receptor stimulates vascular endothelial cell inflammatory responses revealed by transcriptome analysis, PLoS One 8 (2013) e61991.
[10] A. Chen, L. Dong, N.R. Leffler, A.S. Asch, O.N. Witte, L.V. Yang, Activation of GPR4 by acidosis increases endothelial cell adhesion through the cAMP/Epac pathway, PLoS One 6 (2011) e27586.
[11] F. Huang, D. Mehta, S. Predescu, K.S. Kim, H. Lum, A novel lysophospholipid- and pH-sensitive receptor, GPR4, in brain endothelial cells regulates monocyte transmigration, Endothelium 14 (2007) 25–34.
[12] L.V. Yang, C.G. Radu, M. Roy, S. Lee, J. McLaughlin, M.A. Teitell, M.L. Iruela-Arispe, O.N. Witte, Vascular abnormalities in mice deficient for the G protein-coupled receptor GPR4 that functions as a pH sensor, Mol. Cell. Biol. 27 (2007) 1334–1347.
[13] N. Thongon, P. Ketkeaw, C. Nuekchob, The roles of acid-sensing ion channel 1a and ovarian cancer G protein-coupled receptor 1 on passive Mg2+ transport across intestinal epithelium-like Caco-2 monolayers, J. Physiol. Sci. 64 (2014) 129–139.
[14] N. Mohebbi, C. Benabbas, S. Vidal, A. Daryadel, S. Bourgeois, A. Velic, M.G. Ludwig, K. Seuwen, C.A. Wagner, The proton-activated G protein coupled receptor OGR1 acutely regulates the activity of epithelial proton transport proteins, Cell. Physiol. Biochem. 29 (2012) 313–324.
[15] H. Saxena, D.A. Deshpande, B.C. Tiegs, H. Yan, R.J. Battafarano, W.M. Burrows, G. Damera, R.A. Panettieri, T.D. Dubose, S.S. An, R.B. Penn, The GPCR OGR1 (GPR68) mediates diverse signalling and contraction of airway smooth muscle in response to small reductions in extracellular pH, Br. J. Pharmacol. 166 (2012) 981–990.
[16] S. Matsuzaki, T. Ishizuka, H. Yamada, Y. Kamide, T. Hisada, I. Ichimonji, H. Aoki, M. Yatomi, M. Komachi, H. Tsurumaki, A. Ono, Y. Koga, K. Dobashi, C. Mogi, K. Sato, H. Tomura, M. Mori, F. Okajima, Extracellular acidification induces connective tissue growth factor production through proton-sensing receptor OGR1 in human airway smooth muscle cells, Biochem. Biophys. Res. Commun. 413 (2011) 499–503.
[17] I. Ichimonji, H. Tomura, C. Mogi, K. Sato, H. Aoki, T. Hisada, K. Dobashi, T. Ishizuka, M. Mori, F. Okajima, Extracellular acidification stimulates IL-6 production and Ca(2+) mobilization through proton-sensing OGR1 receptors in human airway smooth muscle cells, Am. J. Physiol. Lung Cell. Mol. Physiol. 299 (2010) L567–L577.
[18] J.P. Liu, M. Komachi, H. Tomura, C. Mogi, A. Damirin, M. Tobo, M. Takano, H. Nochi, K. Tamoto, K. Sato, F. Okajima, Ovarian cancer G protein-coupled receptor 1-dependent and -independent vascular actions to acidic pH in human aortic smooth muscle cells, Am. J. Physiol. Heart Circ. Physiol. 299 (2010) H731–H742.
[19] H. Tomura, J.Q. Wang, M. Komachi, A. Damirin, C. Mogi, M. Tobo, J. Kon, N. Misawa, K. Sato, F. Okajima, Prostaglandin I(2) production and cAMP accumulation in response to acidic extracellular pH through OGR1 in human aortic smooth muscle cells, J. Biol. Chem. 280 (2005) 34458–34464.

[20] A.V. Gore, K. Monzo, Y.R. Cha, W. Pan, B.M. Weinstein, Vascular development in the zebrafish, Cold Spring Harbor Perspect. Med. 2 (2012) a006684.
[21] M. Mione, A.H. Meijer, B.E. Snaar-Jagalska, H.P. Spaink, N.S. Trede, Disease modeling in zebrafish: cancer and immune responses–a report on a workshop held in Spoleto, Italy, July 20–22, 2009, Zebrafish 6 (2009) 445–451.
[22] H. Aoki, C. Mogi, T. Hisada, T. Nakakura, Y. Kamide, I. Ichimonji, H. Tomura, M. Tobo, K. Sato, H. Tsurumaki, K. Dobashi, T. Mori, A. Harada, M. Yamada, M. Mori, T. Ishizuka, F. Okajima, Proton-sensing ovarian cancer G protein-coupled receptor 1 on dendritic cells is required for airway responses in a murine asthma model, PLoS One 8 (2013) e79985.
[23] M. Kotake, K. Sato, C. Mogi, M. Tobo, H. Aoki, T. Ishizuka, N. Sunaga, H. Imai, K. Kaira, T. Hisada, M. Yamada, F. Okajima, Acidic pH increases cGMP accumulation through the OGR1/phospholipase C/Ca(2+)/neuronal NOS pathway in N1E-115 neuronal cells, Cell. Signal. 26 (2014) 2326–2332.
[24] O. Murch, M. Abdelrahman, M. Collino, M. Gallicchio, E. Benetti, E. Mazzon, R. Fantozzi, S. Cuzzocrea, C. Thiemermann, Sphingosylphosphorylcholine reduces the organ injury/dysfunction and inflammation caused by endotoxemia in the rat, Crit. Care Med. 36 (2008) 550–559.
[25] E. Afrasiabi, T. Blom, E. Ekokoski, R.K. Tuominen, K. Törnquist, Sphingosylphosphorylcholine enhances calcium entry in thyroid FRO cells by a mechanism dependent on protein kinase C, Cell. Signal. 18 (2006) 1671–1678.
[26] Y. Jin, B.B. Damaj, A.A. Maghazachi, Human resting CD16-, CD16+ and IL-2-, IL-12-, IL-15- or IFN-alpha-activated natural killer cells differentially respond to sphingosylphosphorylcholine, lysophosphatidylcholine and platelet-activating factor, Eur. J. Immunol. 35 (2005) 2699–2708.
[27] J. Qiao, F. Huang, R.P. Naikawadi, K.S. Kim, T. Said, H. Lum, Lysophosphatidylcholine impairs endothelial barrier function through the G protein-coupled receptor GPR4, Am. J. Physiol. Lung Cell. Mol. Physiol. 291 (2006) L91–L101.
[28] Y. Zou, C.H. Kim, J.H. Chung, J.Y. Kim, S.W. Chung, M.K. Kim, D.S. Im, J. Lee, B.P. Yu, H.Y. Chung, Upregulation of endothelial adhesion molecules by lysophosphatidylcholine. Involvement of G protein-coupled receptor GPR4, FEBS J. 274 (2007) 2573–2584.
[29] X. Sun, L.V. Yang, B.C. Tiegs, L.J. Arend, D.W. McGraw, R.B. Penn, S. Petrovic, Deletion of the pH sensor GPR4 decreases renal acid excretion, J. Am. Soc. Nephrol. 21 (2010) 1745–1755.
[30] J.Q. Wang, J. Kon, C. Mogi, M. Tobo, A. Damirin, K. Sato, M. Komachi, E. Malchinkhuu, N. Murata, T. Kimura, A. Kuwabara, K. Wakamatsu, H. Koizumi, T. Uede, G. Tsujimoto, H. Kurose, T. Sato, A. Harada, N. Misawa, H. Tomura, F. Okajima, TDAG8 is a proton-sensing and psychosine-sensitive G-protein-coupled receptor, J. Biol. Chem. 279 (2004) 45626–45633.
[31] K. Seuwen, M.G. Ludwig, R.M. Wolf, Receptors for protons or lipid messengers or both? J. Recept. Signal Transduction Res. 26 (2006) 599–610.
[32] H. Li, D. Wang, L.S. Singh, M. Berk, H. Tan, Z. Zhao, R. Steinmetz, K. Kirmani, G. Wei, Y. Xu, Abnormalities in osteoclastogenesis and decreased tumorigenesis in mice deficient for ovarian cancer G protein-coupled receptor 1, PLoS One 4 (2009) e5705.
[33] T. Nakakura, C. Mogi, M. Tobo, H. Tomura, K. Sato, M. Kobayashi, H. Ohnishi, S. Tanaka, M. Wayama, T. Sugiyama, T. Kitamura, A. Harada, F. Okajima, Deficiency of proton-sensing ovarian cancer G protein-coupled receptor 1 attenuates glucose-stimulated insulin secretion, Endocrinology 153 (2012) 4171–4180.
[34] L. Wyder, T. Suply, B. Ricoux, E. Billy, C. Schnell, B.U. Baumgarten, S.M. Maira, C. Koelbing, M. Ferretti, B. Kinzel, M. Müller, K. Seuwen, M.G. Ludwig, Reduced pathological angiogenesis and tumor growth in mice lacking GPR4, a proton sensing receptor, Angiogenesis 14 (2011) 533–544.
[35] L. Giudici, A. Velic, A. Daryadel, C. Bettoni, N. Mohebbi, T. Suply, K. Seuwen, M.G. Ludwig, C.A. Wagner, The proton-activated receptor GPR4 modulates glucose homeostasis by increasing insulin sensitivity, Cell. Physiol. Biochem. 32 (2013) 1403–1416.

LETTER

doi:10.1038/nature14215

YAP is essential for tissue tension to ensure vertebrate 3D body shape

Sean Porazinski[1]*, Huijia Wang[1]*, Yoichi Asaoka[2]*, Martin Behrndt[3]*, Tatsuo Miyamoto[4]*, Hitoshi Morita[3], Shoji Hata[2], Takashi Sasaki[5], S. F. Gabriel Krens[3], Yumi Osada[6], Satoshi Asaka[2], Akihiro Momoi[6], Sarah Linton[1], Joel B. Miesfeld[7], Brian A. Link[7], Takeshi Senga[8], Atahualpa Castillo-Morales[1], Araxi O. Urrutia[1], Nobuyoshi Shimizu[5], Hideaki Nagase[9], Shinya Matsuura[4], Stefan Bagby[1], Hisato Kondoh[6,10,11], Hiroshi Nishina[2], Carl-Philipp Heisenberg[3] & Makoto Furutani-Seiki[1,6]

Vertebrates have a unique 3D body shape in which correct tissue and organ shape and alignment are essential for function. For example, vision requires the lens to be centred in the eye cup which must in turn be correctly positioned in the head[1]. Tissue morphogenesis depends on force generation, force transmission through the tissue, and response of tissues and extracellular matrix to force[2,3]. Although a century ago D'Arcy Thompson postulated that terrestrial animal body shapes are conditioned by gravity[4], there has been no animal model directly demonstrating how the aforementioned mechano-morphogenetic processes are coordinated to generate a body shape that withstands gravity. Here we report a unique medaka fish (*Oryzias latipes*) mutant, *hirame* (*hir*), which is sensitive to deformation by gravity. *hir* embryos display a markedly flattened body caused by mutation of YAP, a nuclear executor of Hippo signalling that regulates organ size. We show that actomyosin-mediated tissue tension is reduced in *hir* embryos, leading to tissue flattening and tissue misalignment, both of which contribute to body flattening. By analysing YAP function in 3D spheroids of human cells, we identify the Rho GTPase activating protein ARHGAP18 as an effector of YAP in controlling tissue tension. Together, these findings reveal a previously unrecognised function of YAP in regulating tissue shape and alignment required for proper 3D body shape. Understanding this morphogenetic function of YAP could facilitate the use of embryonic stem cells to generate complex organs requiring correct alignment of multiple tissues.

Via exhaustive mutant screening in medaka and zebrafish[5,6], we identified medaka *hir* mutants displaying pronounced body flattening around stage (st.) 25–28 (50–64 h post fertilization, hpf; Fig. 1a). Although general development was not delayed, *hir* mutants exhibited delayed blastopore closure (Fig. 1b, c) and progressive body collapse from mid-neurulation (st. 20, 31 hpf) (Fig. 1d), surviving until just before hatching (6 days post-fertilization, dpf). During body collapse, tissues

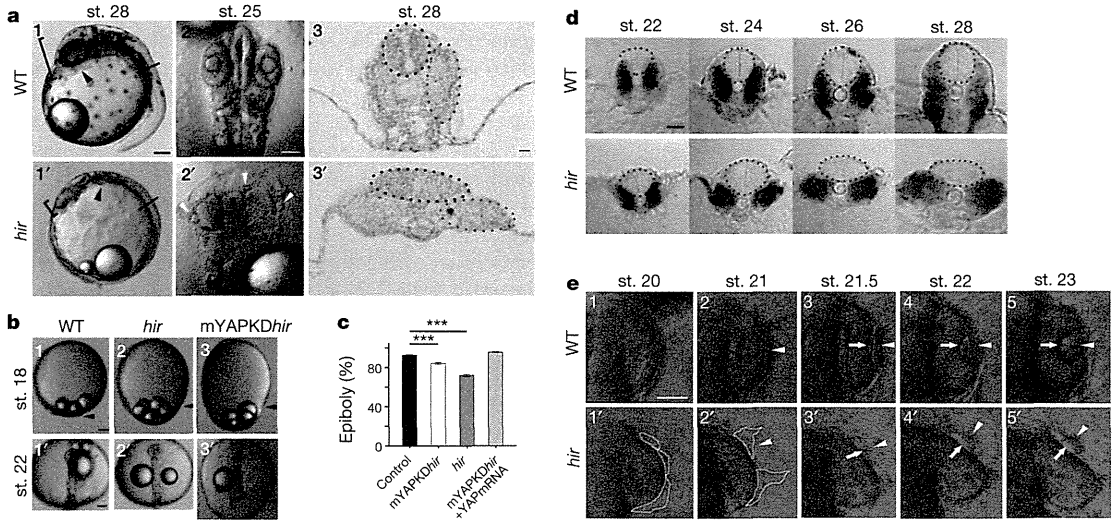

Figure 1 | Organ/tissue collapse and misalignment in *hir* mutants. **a1**, **a1′**, Lateral view of live WT and *hir* mutant embryos, anterior to the left. Arrowheads, heart. Brackets, embryo thickness. **a2**, **a2′**, Dorsal view, anterior upwards. Arrowheads, mislocated lenses. **a3**, **a3′**, Transverse section at the plane shown in **a1** and **a1′**. Neural tubes (black dots) and somites (red dots). **b1**–**b3**, Lateral and **b1′**–**b3′**, dorsal views of live embryos. Arrowheads, blastoderm margin. **c**, Quantification of epiboly (%). Error bars ± s.e.m. (***$P < 0.001$; one-way ANOVA with Dunnett's T3 post hoc. Fig. 1 Source Data). **d**, Transverse sections at 5th somite level, neural tube (encircled) and somites (blue) by *myoD in situ* hybridization. **e**, Time-lapse sequence of dorsal view of WT and *hir* mutant right eyes. Arrowheads, lens placode; arrows, invaginating retina. Fragmented and detaching lens placode demarcated by dotted lines in **e1′** and **e2′**. Scale bars, 40 μm.

[1]Department of Biology and Biochemistry, University of Bath, Bath BA2 7AY, UK. [2]Department of Developmental and Regenerative Biology, Medical Research Institute, Tokyo Medical and Dental University (TMDU), Tokyo 113-8510, Japan. [3]IST Austria, Am Campus 1, A-3400 Klosterneuburg, Austria. [4]Department of Genetics and Cell Biology, Research Institute for Radiation Biology and Medicine, Hiroshima University, Hiroshima 734-8553, Japan. [5]Department of Molecular Biology, School of Medicine, Keio University, Tokyo 160-8582, Japan. [6]Japan Science and Technology Agency (JST), ERATO-SORST Kondoh Differentiation Signaling Project, Kyoto 606-8305, Japan. [7]Department of Cell Biology, Neurobiology, and Anatomy, Medical College of Wisconsin, Milwaukee, Wisconsin 53226, USA. [8]Division of Cancer Biology, Nagoya University Graduate School of Medicine, Nagoya 466-8550, Japan. [9]Kennedy Institute of Rheumatology, Nuffield Department of Orthopaedics, Rheumatology and Musculoskeletal Sciences, University of Oxford, Oxford OX3 7FY, UK. [10]Graduate School of Frontier Bioscience, Osaka University, Osaka 565-0871, Japan. [11]Faculty of Life Sciences, Kyoto Sangyo University, Kyoto 603-8555, Japan.
*These authors contributed equally to this work.